Responses of Rat $P2X_2$ Receptors to Ultrashort Pulses of ATP Provide Insights into ATP Binding and Channel Gating

Luciano Moffatt[1,2] and Richard I. Hume[1]

[1]Department of Molecular, Cellular, and Developmental Biology, University of Michigan, Ann Arbor, MI 48109
[2]Instituto de Química Física de los Materiales, Medio Ambiente y Energía, Consejo Nacional de Investigaciones Científicas y Técnicas, Facultad de Ciencias Exactas y Naturales, Universidad de Buenos Aires, Buenos Aires, 1428, Argentina

To gain insight into the way that $P2X_2$ receptors localized at synapses might function, we explored the properties of outside-out patches containing many of these channels as ATP was very rapidly applied and removed. Using a new method to calibrate the speed of exchange of solution over intact patches, we were able to reliably produce applications of ATP lasting <200 μs. For all concentrations of ATP, there was a delay of at least 80 μs between the time when ATP arrived at the receptor and the first detectable flow of inward current. In response to 200-μs pulses of ATP, the time constant of the rising phase of the current was ~600 μs. Thus, most channel openings occurred when no free ATP was present. The current deactivated with a time constant of ~60 ms. The amplitude of the peak response to a brief pulse of a saturating concentration of ATP was ~70% of that obtained during a long application of the same concentration of ATP. Thus, ATP leaves fully liganded channels without producing an opening at least 30% of the time. Extensive kinetic modeling revealed three different schemes that fit the data well, a sequential model and two allosteric models. To account for the delay in opening at saturating ATP, it was necessary to incorporate an intermediate closed state into all three schemes. These kinetic properties indicate that responses to ATP at synapses that use homomeric $P2X_2$ receptors would be expected to greatly outlast the duration of the synaptic ATP transient produced by a single presynaptic spike. Like NMDA receptors, $P2X_2$ receptors provide the potential for complex patterns of synaptic integration over a time scale of hundreds of milliseconds.

The Journal of General Physiology

INTRODUCTION

P2X receptors are ligand-gated cation channels with no structural similarity to the nicotinic receptor family or to the glutamate receptor family. Their natural agonist is ATP, and $P2X_2$, $P2X_4$, and $P2X_6$ receptors are broadly expressed in the central nervous systems of vertebrates (North, 2002). There is evidence that $P2X_2$ receptors may play a role in certain forms of LTP (Pankratov et al., 2002) and in presynaptic facilitation at synapses onto hippocampal interneurons (Khakh et al., 2003), but the role of purine-gated channels at many synapses in the mammalian central nervous system remains unclear. There is strong evidence that $P2X_2$ receptors are postsynaptic effectors at synapses in the enteric nervous system (Ren et al., 2003).

To understand transmission at puringeric synapses it is important to determine the response of these receptors to pulses of neurotransmitter of duration comparable to those occurring at synapses. Studies of other systems indicate that neurotransmitters reach their receptors at the postsynaptic membrane by diffusion in 0.1 ms or less and their concentration drops with time constants of hundreds of microseconds to a few milliseconds (Land et al., 1984; Reid et al., 1998; Bartoletti et al., 1999; Stiles et al., 1999; Diamond, 2001). The main mechanism determining the dynamics of the neurotransmitter action at the submillisecond time scale seems to be diffusion (Stiles et al., 1999), which depends on the geometry of the synaptic cleft (Bartoletti et al., 1999). At longer time scales enzymatic cleavage is important for terminating the action of acetylcholine (ACh) (Rogers et al., 1966) and ATP (Westfall et al., 1996) while transmembrane transport contributes to clearance of glutamate (Tong and Jahr, 1994), glycine (Zafra et al., 1995), and GABA (Hell et al., 1991). Once neurotransmitter is present at an appreciable concentration, many ligand-gated channels open in the submillisecond range. For instance, $GABA_A$ receptors can open at 1.8–6.7 ms^{-1} (Jayaraman et al., 1999), glycine receptors at 2.2 ms^{-1} (Grewer, 1999), AMPA receptors at 9.5–80 ms^{-1} (Li et al., 2002; Li et al., 2003), and nicotinic ACh receptors at 9.4 ms^{-1} (Matsubara et al., 1992). In contrast, NMDA receptors have been reported to open much more slowly at 0.065 ms^{-1} (Banke and Traynelis, 2003), although single channel analysis suggests that after accounting for preopening states, the actual opening times are much faster (Popescu and Auerbach, 2003). The opening rate of P2X receptors has not been directly measured, although kinetic analysis of $P2X_2$ single channel recordings predicts a value of 1.1 ms^{-1} (Ding and Sachs, 1999).

Correspondence to Luciano Moffatt: lmoffatt@qi.fcen.uba.ar
The online version of this article contains supplemental material.

Abbreviations used in this paper: ACh, acetylcholine; MWC, Monod, Wyman, Changeux.

In this work we developed improved methods for accurately determining the duration of brief applications of transmitter to outside-out patches, and then directly measured the responses of $P2X_2$ receptors to very rapid application and removal of ATP. In addition to providing insight into the expected duration of synaptic responses, these data allowed us to test kinetic models for the transitions between states. These data suggest the presence of an intermediate closed state between the fully liganded channel and the open state, as has recently been suggested for heteromeric glycine receptors (Burzomato et al., 2004). During this intermediate closed state, the ATP is trapped in the binding site and the energetic barrier that precedes the opening of the unbound channel has been significantly lowered.

MATERIALS AND METHODS

Outside-out Patch recording

$P2X_2$ receptors were expressed transiently in human embryonic kidney (HEK) 293T cells. Cells growing in 10 mm diameter wells were transfected with 0.2 μg of a pcDNA3 plasmid driving expression of enhanced green fluorescent protein (EGFP), 2 μg of a pcDNA1 plasmid driving expression of $P2X_2$, and 6 μl of Fugene 6, split the following day over poly-L-lysine–coated coverslips broken into chips with a diameter of ~500 μm, and recorded from 1 or 2 d after splitting. Outside-out patch recordings were obtained using 8–18 MΩ pipettes filled with (in mM) 145 CsFl, 10 EGTA, 10 HEPES, 5 NaCl, and 1.3 $MgCl_2$. EGTA was neutralized with KOH. Patches were clamped at −60 mV with a DAGAN 3900 patch-clamp amplifier (Dagan). The patch clamp head stage was mounted on a Burleigh Model PCS-1000 with a PCS-250 patch clamp driver (EXFO Life Sciences)

ATP (Sigma-Aldrich) was dissolved in the perfusion solution, which contained (in mM) 150 NaCl, 2 KCl, 1.3 $MgCl_2$, 10 HEPES, pH 7.4. We compensated for the chelation of Mg^{+2} by ATP by adding $MgCl_2$ to our solutions such that all solutions contained 1 mM free Mg^{+2}, as determined by the program Bound and Determined (Brooks and Storey, 1992). Currents were low-pass filtered at 10 kHz with a four-pole Bessel filter and digitized at 50 kHz (Digidata 1322A, Axon Instruments). All experiments were done at room temperature (22°C).

Ultrashort pulses generation

The solution switching approach we used was based on the movement of the boundary between two streams of solution of different composition across the tip of the recording micropipette (Fig. 1 A). The movement of the drug application pipette was controlled by a piezoelectric device (Burleigh LSS-3100 Ultra-Fast Solution Switching System, EXFO Life Sciences). When appropriate calibrations were made, this system was capable of moving solution interfaces over the pipette with 10–90% rise or fall times of 100 μs as measured with intact patches. Drugs were applied from 3-barrel square glass pipettes (Warner Instrument) pulled to a barrel width of ~100 μm. Each barrel was connected by PE10 diameter tubing to a micromanifold so that up to four different solutions could be tested. The solution that was allowed to flow was selected by computer controlled pinch valves (BPS-8, ALA Scientific Instruments), and the rate of flow out of the pipette was controlled by applying constant pressure of ~100 torr to the solution reservoirs (2PK+, ALA Scientific Instruments). Once the command signal to the valves was changed, it required ~20 s to change the solution flowing out of the barrel. When a valve was shut and then reopened it required <20 ms to reestablish the flow of that solution and produce a sharp interface between the two solutions flowing out of adjacent barrels.

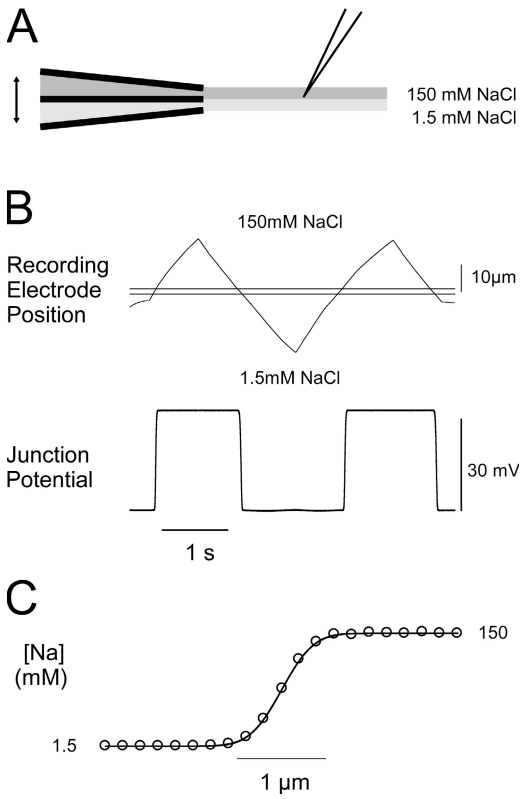

Figure 1. Properties of solution exchange with open-tipped recording pipettes. (A) Diagram of system for rapidly changing the solution bathing outside-out patches. Different solutions flow through the two barrels of the pipette, and outflow is controlled by pressure applied to the solution reservoirs and by the opening and closing of solenoid valves. The arrow indicates the direction of movement of the drug application pipette in response to control pulses from the computer. A second computer controlled a piezoelectric manipulator that could be used to adjust the position of the recording pipette relative to the solution interface. (B) The change in junction potential when the solution boundary between 150 mM NaCl and 1.5 mM NaCl was moved across the recording pipette at low speed (40 μm/s). The 33-mV shift indicates that these data are as predicted from the Henderson equation. (C) The junction potential measured at closely spaced distances indicated that the 10–90% range of the concentration profile is ~0.7 μm.

One important factor that affects the speed of solution exchange is the position of the recording pipette relative to the drug application pipette. The tip of the recording pipette was held perpendicular to the flow of solution by the placement of the micromanipulators on the table. The height of the recording pipette tip was set ~17 μm below the bottom of the septum of the drug application pipette by using the calibrated focus knob on the microscope, and the lateral distance between the drug application pipette and the recording pipettes was set to ~17 μm by a reticule in the eyepiece. As the drug application pipette entered the solution at ~45° this placed the recording tip ~25 μm straight ahead of the septum.

As one approach to calibrating the drug application system, small movements of the liquid boundary were detected by changes in the liquid junction potential at the open tip of a pipette located

near the interface between solutions. In these experiments, the recording pipette was filled with internal recording solution while the drug application barrels contained 150 mM NaCl and 1.5 mM NaCl, respectively (Fig. 1 B). The expected junction potential of the pipette tip relative to the test solution should be described by the Henderson formula (Barry and Lynch, 1991):

$$V_{IO} = -\frac{RT}{F}\frac{\sum_i z_i u_i \left(c_{iO} - c_{iI}\right)}{\sum_i z_i^2 u_i \left(c_{iO} - c_{iI}\right)} \ln\left(\frac{\sum_i z_i^2 u_i c_{iI}}{\sum_i z_i^2 u_i c_{iO}}\right), \qquad (1)$$

where V_{IO} is the junction potential between the solution I and J, z_i, and u_i refers to the valence, mobility, and concentration of each one of the ions present at each side of the boundary. When the drug application pipette was held fixed, and the recording pipette moved very slowly across the boundary (~30 μm/s, Fig. 1 B), the junction potential was in equilibrium at all points. In this way the boundary was measured and the concentration profile calculated. As expected, the potential difference between the two solutions was ~33 mV and changes in the concentration across the boundary could be described by the error function (Sachs, 1999). These experiments indicate that at the rate of solution flow we used, the boundary had a 10–90% width of 0.7–0.9 μm (Fig. 1 C).

To improve the temporal resolution of the solution switcher we measured the solution exchanger vibrational dynamics. In this way we could minimize the mechanical vibrations induced in the piezo-stage and application pipette, which otherwise can lead to multiple undesired transitions of the solution across the patch (Stilson et al., 2001). The dynamics of the solution exchanger were modeled by its transfer function, which was experimentally determined by the methods of Stiltson et al. In brief, we measured the potential changes due to the movement of the liquid boundary across the open tip of a pipette after the application of 200 μs square voltage pulses of various amplitudes to the piezo translator when the recording tip was positioned at a variety of locations relative to the solution interface. Once the transfer function was calculated from these data, the optimal input (i.e, the voltage applied to the piezo-stage) for any desired output was calculated by the methods previously described (Stilson et al., 2001). The command stimulus necessary to produce a 200-μs response was quite complex, beginning and ending many milliseconds before and after the detectable movement (Fig. 2 A).

The final adjustment of the recording pipette relative to the solution interface was done as illustrated in Fig. 2 B. We changed the position of the recording pipette in 0.67-μm steps by changing the voltage coming into the X axis controller of the micromanipulator that held the patch clamp head stage (Model PCS-1000 with a PCS-250 patch clamp driver, EXFO Life Sciences). Responses to a constant stimulus delivered to the drug application piezo at 12 different positions of the recording pipette are shown in Fig. 2 B. As the pipette was placed more distant from the interface, the latency until a detectable response was observed got longer, the duration of the response got shorter, and finally the response ceased to reach a level equal to the full junction potential produced by the low NaCl solution. From the increase in latency (~180 μs over the 8-μm displacement, Fig. 2 B, dashed lines) the velocity of the moving boundary can be estimated to be 45 μm/ms. As the interface thickness was shown above to be ~0.7 μm, the predicted 10–90% rise time is 16 μs. However, at the position that produced a response lasting ~200 μs (thick line) the actual 10–90% rise time was ~85 μs (Fig. 2 C).

Our data were usually filtered at 10 kHz with a 4-pole Bessel filter, so it was possible that this filter was the cause of the unexpectedly slow response. One approach to test this was to simply set the filter to a higher cutoff frequency, while a second approach was to simulate the effect of a Bessel filter using Matlab. Both approaches

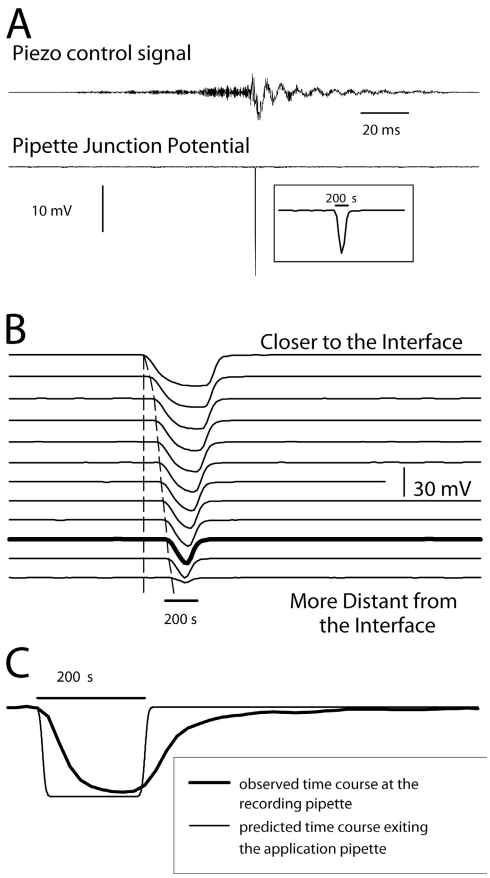

Figure 2. Movements of the solution boundary between 150 and 1.5 mM NaCl can be made very rapidly. (A) The optimal command potential to the piezo driver moving the drug application pipette necessary to damp out vibrations was complex. The top traces show the command potential, and the bottom trace shows a single sharp spike in the junction potential. The time course of the junction potential waveform at higher temporal resolution is illustrated in the inset box. (B) The pipette junction potential in response to a fixed stimulus to the piezo controlling the position of the drug application pipette is plotted for 12 different positions of the recording pipette. In all cases the recording pipette began in the 150 mM NaCl solution and the initial potential was 0 mV. The top trace was obtained when the recording pipette was close to the boundary, and each subsequent trace was 0.67 μm more distant. The heavy black trace indicates a position where this stimulus produced a pulse lasting ~200 μs. The dashed lines indicate the difference between the latency until a response began at the position closest to the boundary and the beginning of a response in each subsequent trace. The velocity of the piezo movement was estimated from these lines to be ~45 μm/ms. (C) Predicted and observed time courses of the solution exchange. The thin line indicates the concentration profile expected based on a velocity of the piezo of 45 μm/ms. The thick line indicates the concentration profile actually obtained, and was calculated from the thick trace in B using the Henderson equation.

demonstrated that at most 7 μs of the increase in rise time was due to the filter. A plausible explanation for the slower than expected rise time of the optimized response is that ions have to diffuse over the unstirred layer created at the tip of the pipette (Sachs, 1999). The region around the patch is subject to both convection and diffusion. Diffusion of different molecules varies

according to size, the diffusion coefficient of Na being approximately five times faster than that for ATP. A slower diffusion coefficient also steepens the gradient across the boundary and increases the time needed to cross the unstirred layer at the tip of the recording pipette. To estimate the contribution of both effects we simulated the expected changes in the concentration seen at the patch using a numerical integration of the convection diffusion equation: $\vec{v} \cdot \nabla C - D\nabla^2 C = -\partial C / \partial t$, where $\vec{v}$ is the vector velocity of the fluid, C is the concentration, and D is the diffusion coefficient. We solved the result for the one-dimensional case along the axis in which the drug application pipette moves. Following results of Sachs, we assume that velocity is maximal up until one reaches a distance of approximately three times the radius of the patch, and that the velocity comes to 0 at the patch (Fig. 3 A). To simulate conditions close to our experiments we set the initial distribution to be the result of crossing the 0.7-μm boundary at 45 μm ms^{-1} (Fig. 3 B). We set the distance between the exit point of the drug application pipette and the patch to be 25 μm (since it was the position set in the actual experiments), and by adjusting the parameters representing the velocity and the radius of the pipette (which determine the shape of the velocity field near the patch) we found a good agreement with the data using a velocity of 60 μm ms^{-1} and a patch radius of 1.2 μm (Fig. 3 B). At the exit point of the drug application pipette the rise time is ~16 μs and it begins with no delay. It requires ~350 μs for the concentration change to begin 20 μm away, and the rise time remained rapid (~30 μs) for both sodium and ATP. It takes ~150 μs to travel the last 5 μm, where the velocity of the fluid drops to zero. The rise time decreases to ~100 μs with the predicted exchange of ATP delayed by ~20 μs with respect to the exchange of Na.

Experimental Protocols

Application of high concentrations of ATP for hundreds of milliseconds resulted in desensitization. Furthermore, the responses of outside-out patches containing $P2X_2$ receptors ran down over time. To deal with these complications, we tested patches no sooner than 1 min after the previous stimulus and sandwiched each test concentration between two normalizing stimuli (1 mM ATP for 10 ms). The amplitude of the test response was then normalized to the average of the two normalizing responses. With this paradigm, the variability in amplitude between successive normalizing responses (spaced 2 min apart) was <10% in most trials. Trials in which the amplitude of the normalizing responses changed by >10% were not included in the analysis.

Data Analysis, Kinetic Modeling, and Statistical Analysis

We used custom written functions in MATLAB 6.5 for fitting the data. For fitting exponential functions or exponential matrices we used the built in function lsqrnonlin, using the options "Large-Scale on" and "LevenbergMarquardt on." We fed the algorithm with the raw data during the pulse but averaged the data at logarithmically spaced intervals (10 points per decade) after the pulse ended. In this way we reduced the size of the data vector from 200,000 to 100, without losing significant information, allowing us to rapidly fit large datasets and complex models. In some cases, the fit was forced to obey a particular constraint (that the EC_{50} matched the experimentally obtained value) by adding a penalty to the squared sum when the constraint was not matched. To get estimates of the standard errors in the parameter determinations we used a bootstrapapproach (Kraushaar and Jonas, 2000). A balanced resampling was obtained by concatenating 100 copies of the original set of traces and generating a random permutation of the all $100*n_{traces}$. Subsequently, 100 bootstrap replications were read as successive blocks of length n_{traces}. Each bootstrap replica was refitted using the best fit values of the original traces set as the initial values. Errors were estimated from percentile intervals.

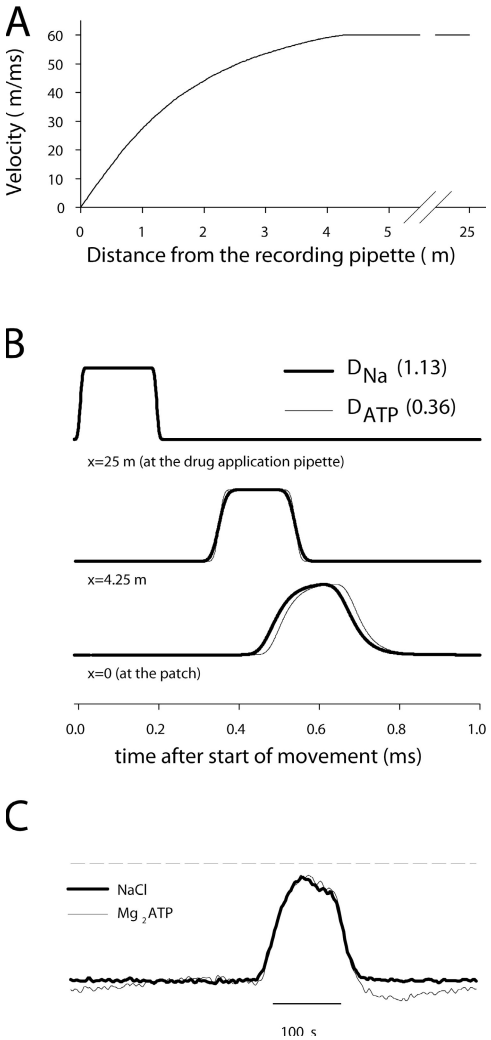

Figure 3. Numerical analysis of the predicted concentration profile at the recording pipette based on the one-dimensional diffusion-convection equation. (A) Velocity as a function of the distance from the tip used for the numerical integration. The maximal velocity is the fluid velocity (v). These data were obtained from a two-dimensional integration of the Bernoulli equation by Sachs (1999) and represent the values that would be obtained for a recording pipette with a radius of 1.2 μm. (B) The predicted time course of appearance and disappearance of ATP and Na in response to stimulus that produces a 200-μs duration response at the patch. The amplitudes of all responses are normalized to 100% of the maximum response at that point. The parameters used for the fit were diffusion $coefficient_{Na}$ = 1.133, diffusion $coefficient_{ATP}$ = 0.36, fluid velocity = 60 μm/ms, recording pipette radius = 1.2 μm. (C) The measured time course of the open tip junction potential as the NaCl concentration or the MgATP concentration increased and decreased between 1 and 10 mM. The junction potential values were normalized to facilitate their comparison. The dashed line indicates the maximum amplitude of the junction potential for a long pulse.

Online Supplemental Material

Different aspects of the kinetic analysis are described in detail in the online supplemental material (available at http://www.jgp.org/cgi/content/full/jgp200709779/DC1). The supplemental material includes two approaches to the kinetic analysis of Scheme 1,

(1) split analysis and (2) global fitting; also, it contains (3) a discussion over the performance of the discarded Schemes 2 and 3 and (4) the parametrization procedure of allosteric model Schemes 6 and 7. Moreover, four supplemental figures are provided: (Fig. S1) the fits to all explored models replotted in a linear amplitude axis; (Fig. S2) an expanded view of Scheme 6; and (Figs. S3 and S4) expanded views of Scheme 7.

RESULTS

Exchange Time on Intact Patches

When recording pipettes with outside-out patches were placed at the position that our experiments on open-tipped pipettes suggested would yield optimized responses, we found a striking variability between patches in the rise time kinetics of recombinant $P2X_2$ receptors. For the majority of patches exposed to 1 mM ATP, the 10–50% rise time was <1 ms, but in some patches it was 5 or even 10 ms and the response began with a substantial delay (Fig. 4). All of these patches were ruptured at the end of the experiment and the speed of exchange measured based on the open tip junction potential was uniformly rapid, confirming that the recording pipettes were properly positioned. We also found that for some patches, the time course of the response to 1 mM ATP changed dramatically over time. We hypothesized that the large outside-out patches that we made in order to obtain currents of sufficient magnitude might sometimes partially fold over on themselves, and thus impede solution exchange. We therefore developed a method for estimating the speed of solution exchange that could be performed on intact patches expressing $P2X_2$ receptors.

The intact patch calibration method first opens the $P2X_2$ channels with ATP and then alters the cation composition of the solution, replacing most of the Na^+ with $NMDG^+$, which is much less permeable than sodium. When ATP is present continuously, changes in the current arise not because of any conformational change in the $P2X_2$ channel but because of the changes in the concentration of extracellular Na that reach the channel. The published literature indicates that P_{Na}/P_{NMDG} is 0.03 following brief applications of ATP to oocytes or HEK293 cells, but can increase to 0.12 if prolonged application of ATP allows the channel to enter the megapore state (Khakh et al., 1999; Virginio et al., 1999). The changes in current observed after the exchange of Na for NMDG should be described by the Goldman-Hodgkin-Katz equation:

$$I_X = P_X \cdot z_X{}^2 \cdot \frac{E \cdot F^2}{RT} \cdot \frac{[X]_{int} - [X]_{ext} \cdot \exp(-z_X FE/RT)}{1 - \exp(-z_X FE/RT)}, \quad (2)$$

where P_x is the membrane permeability for the ion x, E is the membrane potential, and $[X]_{int}$ and $[X]_{ext}$ are the concentration of the ion x at the internal and external side of the patch. For constant membrane potential and permeability, the equation states that the total current is a linear function of the concentration of sodium and NMDG. That means that the measured current is a linear function of the extent of solution switching.

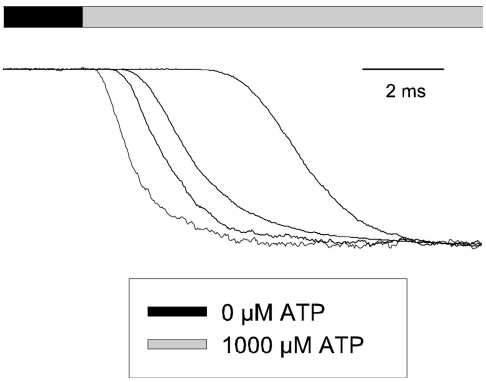

Figure 4. Variability in the rate of rise in ATP-evoked currents. The responses were normalized so that they all reached the same maximal amplitude. For all four patches, the junction potential obtained after the patch was ruptured was very rapid, indicating that the recording pipettes had been correctly placed relative to the solution boundary.

The results of an on-patch assessment of the speed of solution exchange are presented in Fig. 5. Because we were limited to rapidly switching between only two barrels, the actual experimental protocol was slightly more complex than would be necessary if rapid switching between three solutions were possible. In this experiment, one barrel contained standard sodium containing external solution with no ATP, while the other barrel contained 100 μM ATP in NMDG external solution. The patch was placed on the side of the interface containing no ATP. About 200 ms before each trace, the flow from this barrel was temporarily shut off by a computer-controlled valve. This allowed the solution coming out of the ATP containing barrel to mix at the patch, so the solution initially bathing the patch was an undefined mixture that contained a sufficient amount of ATP to open many channels and sufficient sodium to drive an inward current. 35 ms before the beginning of each trace, flow was reinitiated through the 0 ATP barrel. This returned the patch to a 0 NMDG, 0 ATP environment within 10 ms, but because the time constant of decay of the ATP-activated currents following ATP removal is >50 ms, inward currents were readily observed for a few hundred milliseconds until the currents returned to baseline. When the solution was transiently switched to the ATP-NMDG solution for 10 ms (Fig. 5 A) the current at −60 mV rapidly decreased to close to 0 due to the change in driving force, and then rapidly returned to a substantial inward level when the sodium-containing solution was reapplied. The inward current at the end of this pulse was greater than at the beginning of the pulse because 10 ms was a sufficient period of time for the increase in ATP during the ATP-NMDG pulse to open more channels.

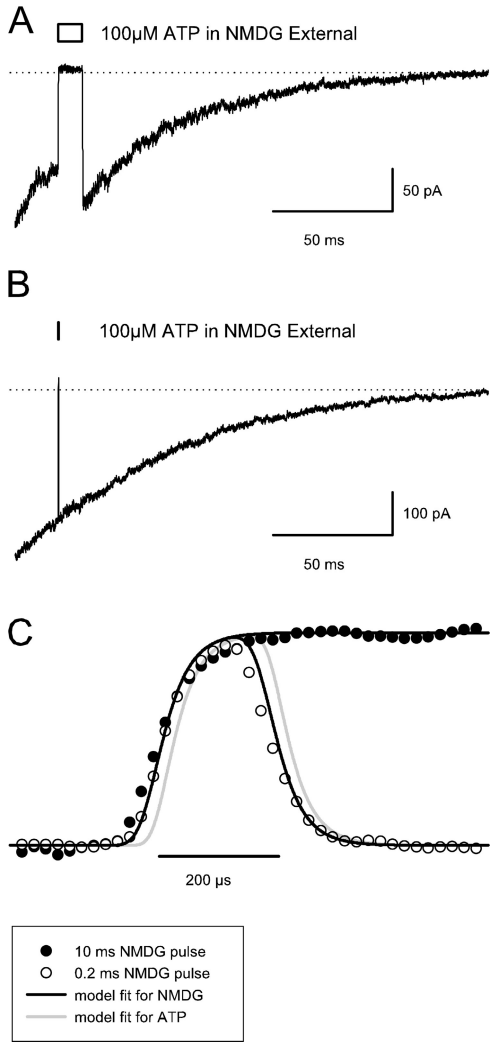

Figure 5. Demonstration of the method used to determine the speed of solution exchange on intact patches. One barrel of the drug application pipette contained normal sodium external solution without ATP and the other contained NMDG external solution with 100 μM ATP. (A) Just before the start of the trace the patch was switched out of a solution containing a mixture of NMDG and sodium solutions with ATP into the sodium solution without ATP, so that many channels were open and there was a significant inward driving force but no ATP was present. At the time indicated by the box, the patch was shifted into the NMDG solution with 100 μM ATP for 10 ms, and then back into the sodium containing solution with no ATP. (B) The procedure was the same as in A but the NMDG pulse lasted only 0.2 ms. (C) Time detail of both pulses. The currents were normalized to facilitate comparison. The peak current reduction in response to the 0.2-ms pulse (open circles) was 93% of the reduction in the 10-ms pulse (filled circles). The black lines show the expected time course of the responses to NMDG after integrating the convection-diffusion equation. For times longer than 200 μs after the start of the pulse, the black line predicting the response to the 10-ms pulse is obscured by the gray line predicting the response to a 10-ms pulse of ATP. We optimized the parameters r (radius of the pipette) and v (velocity of the fluid coming out of the application pipe) to obtain the best fit. The gray lines show the deduced time course of the ATP concentration by integrating the same equation with the same parameters except using the diffusion constant for ATP.

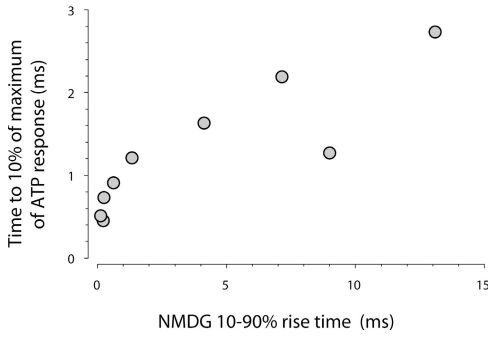

Figure 6. Scatterplot demonstrating that a slow rate of exchange can account for the patches in which the response to ATP was slow.

In contrast, when the stimulus to the solution switcher produced a pulse of only 200 μs (Fig. 5 B) the inward current also transiently decreased to near 0, but no increase in the inward current after the pulse was observed. The 10–90% rise time of the NMDG pulse was ~90 μs (Fig. 5 C), very similar to the rise time for the exchange of sodium on open pipette tips shown in Fig. 2.

The importance of carrying out the on-patch calibration technique to assess the speed of solution exchange rather than testing the open tip exchange rate at the end of the experiment is illustrated by data presented in Fig. 6. Every patch that responded slowly to ATP (i.e., took longer than 1 ms to reach 10% of the maximum response to ATP) also showed a slow 10–90% rise time in response to NMDG. This indicates that slow solution exchange, and not complex properties of channel gating, was responsible for the slow rising responses; thus data from slow patches needed to be eliminated before kinetic analysis.

Responses of $P2X_2$ Receptors to Submillisecond Pulses of ATP

The on-patch method for assessing the speed of exchange was applied every few minutes to each patch being considered for kinetic analysis. Data were considered to be from a slow patch and excluded from analysis if the 10–90% exchange rate of NMDG was >150 μs or if the amplitude of the response to a 1-ms application of a saturating concentration of ATP was <90% of the response to a long application of the same concentration of ATP. Only ~20% of the patches passed these initial tests, and most of these patches showed an unacceptable slowing of the exchange rate over time, or broke before a full dataset could be collected. For six patches, solution exchange remained sufficiently rapid for the entire period of data collection to carry out a complete kinetic analysis of the responses to a range of ATP concentrations.

The responses of a single patch to 200-μs pulses of increasing ATP concentration (0.1–10 mM) are shown in Fig. 7 A with the rising phase shown at higher temporal

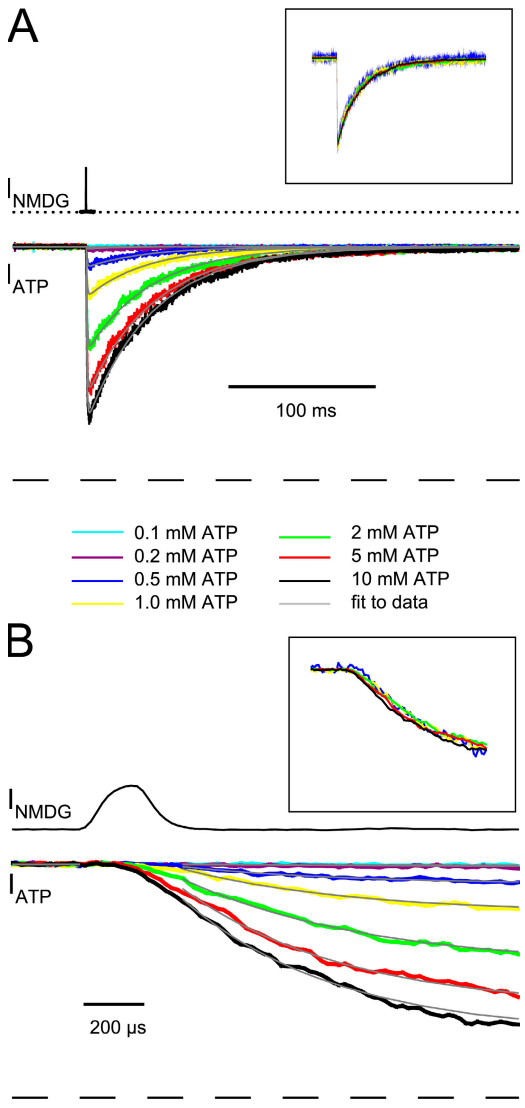

Figure 7. Response of a patch expressing $P2X_2$ receptors to the application of 200-μs pulses of ATP at 0.1, 0.2, 0.5, 1, 2, 5, and 10 mM. The membrane potential was held at −60 mV. (A) The top trace shows the time course of the response to a 200-μs pulse of NMDG external solution (as in Fig. 5), to test the speed of solution exchange. The lower set of colored traces are the current responses to the indicated concentrations of ATP and the smooth gray traces are the fits of Eq. 5 to these data. The amplitude of the traces was normalized to the amplitude of 10-ms pulses of 1 mM ATP (which evoked maximal amplitude of response). The inset shows the current responses for 500 μM and greater concentrations normalized to the same peak amplitude. (B) The same data as in A shown on a much more rapid time scale.

resolution in Fig. 7 B. Four features of the kinetics of these responses are of particular importance to understanding the mechanism of activation and deactivation of $P2X_2$ receptors. First, when the responses to different concentrations were normalized to the same peak amplitude, the entire time course of the responses to concentrations of 500 μM and greater were superimposable (see the insets of Fig. 7, A and B). This indicates that the time course of the ATP concentration change at the patch was as brief as expected based on the diffusional profile of NMDG exchange for Na on the same patch. Second, there was a significant amount of ATP-activated current for several hundred milliseconds after all of the ATP had been washed away. Third, most of the rise in the ATP-activated current occurred after the free ATP concentration had fallen back to 0. The peak current was not achieved until 3–4 ms after the ATP pulse had ended. Fourth, there was a delay of ∼100 μs between the time when ATP arrived at the receptors and the first detectable flow of inward current.

To analyze the amplitude of responses, it was necessary to compensate for the slow rundown of responsiveness, as described in Materials and Methods. When this was done, the peak response to the 200-μs pulses could be shown to increase with the concentration of ATP until saturation was reached at ∼10 mM. Two features of the concentration response relation to ultrabrief pulses are of particular interest. First, although 100 μM ATP produced a maximal response when applied for 200 ms or longer, it barely induced any response when applied for 200 μs. Second, the amplitude of the saturating response to 200-μs pulses reached only 70% of what was achieved by applying 1 mM ATP for 10 ms (the dashed 100% line in Fig. 7, A and B).

One possible explanation for observing a difference in amplitude in the responses to very brief or long pulses of the saturating level of ATP might be that the channel is blocked by a high concentration of ATP in the same way ACh receptors are blocked by a high concentration of acetylcholine. An open channel blocking mechanism seemed unlikely, as <5% of the current had occurred by the end of the 200–300-μs period when the ATP was present (Fig. 7 B), and could be ruled out because were this the case, the responses to brief pulses would have been larger, with the steady-state amplitude representing both channel activation and block.

The explanation we favor for the increased efficacy of long pulses is that the responses to very short pulses are limited by the trapping efficiency of the channel. We define trapping efficiency as the probability that a fully bound channel opens at least once before the agonist leaves the channel.

$$\Pi = P\begin{pmatrix}\text{exit to fully bound open state}/\\ \text{start in closed fully bound state}\end{pmatrix} \qquad (3)$$

Stated in another way, after ATP is bound to the channel it can leave the channel without causing any openings, or it becomes trapped and then the channel eventually opens one or more times. If the duration of the pulse of ATP is much shorter than the mean unbinding time, then the ratio of the current in response to a very short pulse to the current in response to a much longer pulse reflects only the trapping efficiency.

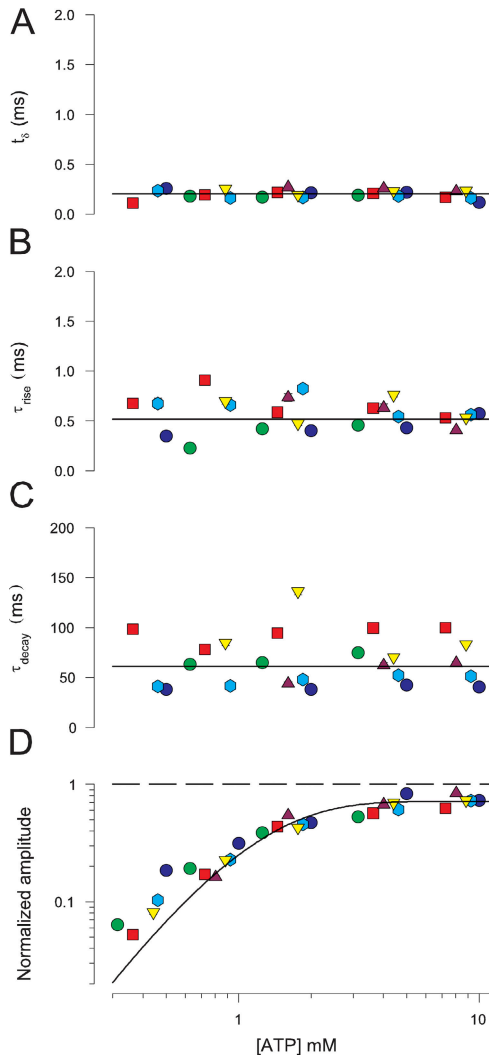

Figure 8. Responses to 200-μs pulses of ATP at a variety of different concentrations from six different patches. The ATP-evoked current from each trace was fit to Eq. 4, and the parameters from the fit (t_δ, τ_{rise}, τ_{decay}, and A) were plotted as a function of the normalized concentration of ATP. Each point represents a single response; each symbol represents a different patch. Time delay (t_δ) was measured from the start of the pulse (defined as the time when 10% of the response to NMDG was reached) to the time when the back-extrapolated rising exponential current in response to ATP was zero. Normalized ATP concentration was calculated by multiplying the ATP concentration by a scaling factor equal to the duration of the brief NMDG calibration pulse (in μs) divided by 200 μs.

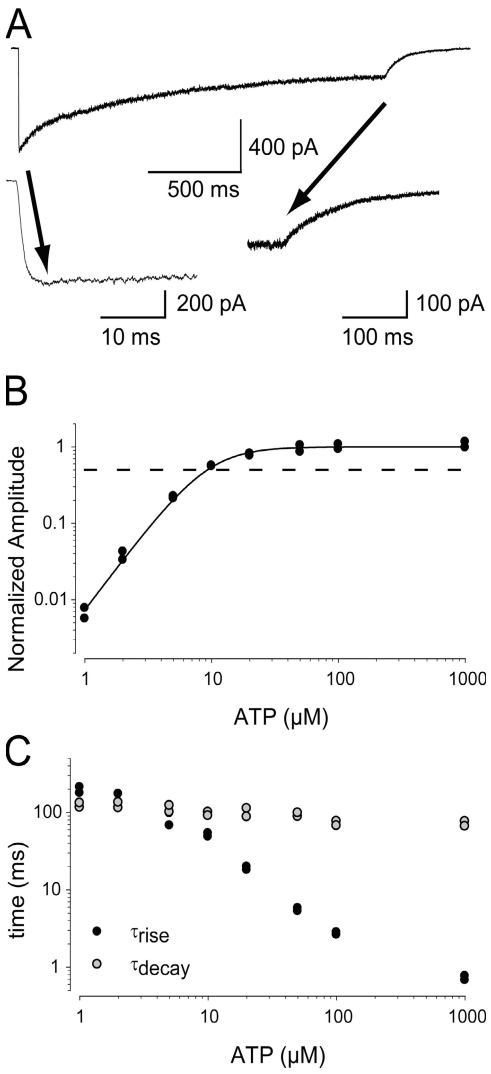

Figure 9. Responses of a single patch to long pulses of ATP at a variety of ATP concentrations. (A) Trace of one patch in response to a 2-s application of 1,000 μM ATP. The two bottom traces show portions of the full trace at higher time resolution. Desensitization was negligible in the first 20 ms of the response, but was apparent at longer times, with a time constant of ~620 ms. The deactivation after ATP was removed was much slower than the onset of the ATP response. (B) Peak current as a function of ATP concentration for long pulses of ATP. The dashed line represents the maximal current that could be obtained for a 200-μs pulse of 10 mM ATP. (C) The time constant of the rising and falling phases of the response to long pulses of ATP at various concentrations.

We interpret our results in that sense; for 200-μs pulses that saturated the receptor with ATP, 30% of the time the agonist left the receptor without inducing a single opening.

The responses once ATP had fallen to a negligible level were well described by a biexponential function with a delay (see gray lines in Fig. 7, A and B):

$$y(t) = A \cdot \left(\exp\left(-\frac{t - t_\delta}{\tau_{decay}} \right) - \exp\left(-\frac{t - t_\delta}{\tau_{rise}} \right) \right). \quad (4)$$

This function has four parameters: the amplitude A, the time constants of rise τ_{rise} and decay τ_{decay}, and a time delay t_δ, which indicates the time when the back-extrapolated current is zero. To estimate these parameters we fitted the responses for six patches (depicted by different symbols) to nominal 200-μs applications of ATP at concentrations up to 10 mM (Fig. 8). As the exact width of the ultrashort pulses varied between experiments performed on different patches (but the variability of the pulses for the same patch was always <10%), we adjusted

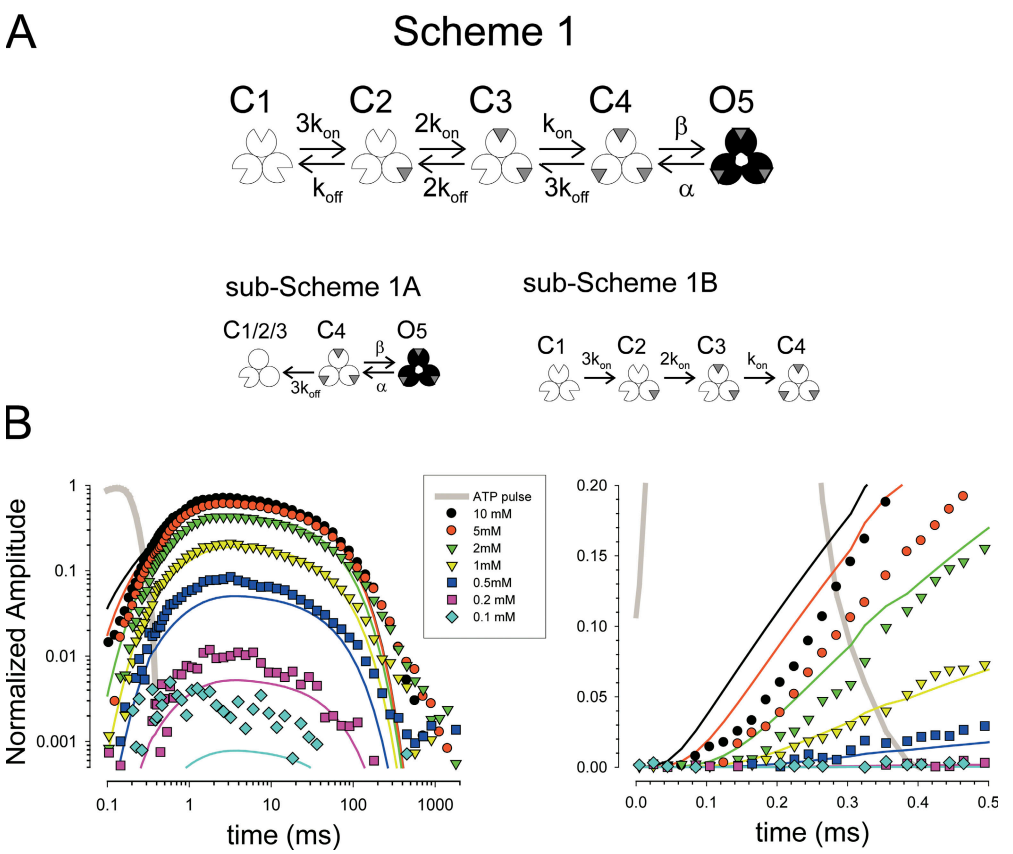

Figure 10. Initial kinetic analysis. (A) Minimal linear scheme for a homotrimeric channel in which all binding sites must be occupied before channel opening can occur. Sub-Scheme 1a represents the possible transitions once all of the ATP has been washed away, and sub-Scheme 1b represents the transitions that will occur during an ultrashort pulse if β and $3K_{off}$ are slow relative to the duration of the pulse. (B) The global fitting of data to Scheme 1. The colored lines match the data points of the same color. The gray line represents the predicted time course of ATP based on the time course of the response to an NMDG pulse. The full dataset is shown on log axes on the left, and the earliest phase of the responses is shown on linear coordinates on the right.

the values of the concentrations by multiplying them by a scaling factor equal to the duration of the NMDG calibration pulse (in μs) divided by 200 μs.

The time constants and delay time did not systematically vary with the applied ATP in the analyzed range (Fig. 8, A–C), confirming that the application of ATP was essentially instantaneous relative to the kinetics of these channels. However there was some variability in the value of the time constants among different patches. For the rise time the coefficient of variation was of 27% between patches and 23% within the same patch (n = 36 traces, 3–14 per patch); for the decay time, the coefficient of variation was 44% between patches and 17% within the same patch, and for the delay time, 16% between patches and 23% between traces of the same patch. The average value for the delay time t_δ was 0.20 ms, for τ_{rise} was 0.57 ms, and for τ_{decay} was 62.4 ms.

In contrast to the concentration independence of the kinetic properties of the responses to ultrashort pulses, the amplitude of the response increased sharply as concentration was increased and saturated at ~70% of the amplitude in response to a long application of ATP (Fig. 8 D). The slope of this relation suggests that more than one ATP must be bound to efficiently open the channel. According to this idea, the smaller peak current at lower concentrations occurs because fewer and fewer receptors were able to bind a sufficient number of ATP molecules to open with high probability. Assuming that the purinergic receptor is a trimer (North, 2002), as an initial model we can postulate a sigmoid function that is the sum of three exponential functions described by the equation

$$A(x) = A_{\max}\left(1 - \exp(-3k_a \cdot x) + 3 \cdot \exp(-2k_a \cdot x) - 3 \cdot \exp(-k_a \cdot x)\right), \quad (5)$$

where x is the integral over time of the ATP concentration during the pulse. This equation has only two parameters to fit: the saturating amplitude A_{max} and the apparent association constant k_a. The fit of the data to this equation was excellent at high and medium concentrations, but there was a noticeable deviation at the lowest concentrations, where the currents were larger than predicted. This discrepancy will be addressed in the second part of the Results.

For ATP concentrations of 200 μM or greater (the range used in the experiments with 200-μs pulses), 10 ms was sufficient to produce responses that reached the peak amplitude, yet short enough to elicit negligible desensitization (Fig. 9 A). For longer applications of high concentrations of ATP there was obvious desensitization with a time constant of 628 ± 13.4 ms (n = 6). The steady-state concentration response relation revealed by 2-s pulses had an EC_{50} of 9.8 μM and a Hill coefficient of 1.8 (Fig. 9 B). The rise time for long pulses was a steep function of ATP concentration, with the time constant decreasing from over 100 ms at low concentrations

TABLE I
Kinetic Analysis of the Experimental Data under Scheme 1

	a. Split Scheme 1 analysis	b. Global Scheme 1 analysis
Macroscopic parameters		
τ_{rise} (ms)	**0.518 ± 10.0%**	0.788[a]
τ_{decay} (ms)	**61.3 ± 17.2%**	56.3
t_δ (ms)	**0.203 ± 0.007**	0.094[a]
A_m	**0.714 ± 0.018**	0.68
k_a (s^{-1} μM^{-1})	**6.09 ± 5.7%**	6.29
EC_{50} (μM)	16.3	14.9
kinetic rates		
k_{on} (s^{-1} μM^{-1})	6.09 ± 5.7%	**6.73**
k_{off} (s^{-1})	212 ± 12.5%	**166**
α (s^{-1})	54.3 ± 19.8%	**45.3**
β (s^{-1})	1681 ± 12.5%	**743**
Microscopic constants		
Π	0.690	0.600
Km (μM)	31.7	24.6
E	24.2	16.4

Values of macroscopic parameters, kinetic rates, and microscopic constants obtained from six patches by using a split analysis or a global analysis. In the first case we obtained the macroscopic parameters from the experimental data (in bold); the kinetic rates were calculated from the macroscopic parameters. In the second case we obtained the kinetic rates directly from the experimental data (starting 0.5 ms after the application of the ATP pulse) by running a nonlinear algorithm. The estimated rates from this fit are shown (in bold). The macroscopic parameters and the microscopic constants were calculated from these kinetic rates.
[a]Parameter that differs significantly between the two fits.

to 0.72 ms at 1 mM (Fig. 9 C). This latter value is quite similar to the time constant of the rise in response to 200-μs pulses of saturating levels of ATP. The time constant of the falling phase after ATP was rapidly washed away was independent of the concentration of ATP and averaged 99 ms, which is within the range observed for patches studied with brief pulses.

Initial Kinetic Analysis of Rapid Application Data

In this second half of the Results we interpret the results of the responses to 200-μs pulses in terms of plausible mechanisms for the agonist action. $P2X_2$ receptors are homotrimers, so it is expected that in the absence of ATP they have three identical unoccupied ATP binding sites. We therefore began our exploration of potential mechanisms of receptor activation with Scheme 1 (Fig. 10), which postulates that the channel opens in a single step subsequent to the binding of ATP to all three sites, and that there is no change in a binding site as a consequence of ATP binding at other sites. This model has only four parameters, which by the usual convention are referred to as binding rate (k_{on}), unbinding rate (k_{off}), opening rate (β), and closing rate (α). To estimate the parameters that best fit this model, we took two approaches. The first approach was a split analysis based on the plausible simplifying assumption that if the pulse of ATP is sufficiently rapid relative to α, β, and k_{off}, then all that happens during the pulse is that some channels get provisioned with ATP, but no channels open. On this assumption, the time course of the response is determined entirely by sub-Scheme 1a, while the amplitude of the response is determined primarily by sub-Scheme 1b (Fig. 10). The second approach used a global fitting method that made no assumptions about the relation between parameters. Details of both analytical approaches are available in the online supplemental material (available at http://www.jgp.org/cgi/content/full/jgp.200709779/DC1). Table I shows the results of both approaches for the mean of six patches. The rate constants obtained by both approaches differed by <20% except for the opening rate, where the values obtained by the global analysis were ∼50% of those obtained from the split analysis. The binding rate at the maximal ATP concentration used (k_{on} * 10 mM ATP) was 36 times faster than the opening rate. The unbinding rate was about eightfold slower than the channel opening rate, and the closing rate was ∼30-fold slower than the opening rate. At 10 mM ATP, these parameters predict that 99% of the receptors will have all three ATP sites occupied by 100 μs.

Further Kinetic Analysis

When we used the parameters of the global fit to Scheme 1 to predict the time course of the currents, there was good agreement in τ_{decay} and in A_{max}, but the measured delay time was about twice as long as the predicted value of ∼100 μs, and the experimentally measured rise time was quite a bit faster than the predicted rise time (∼200–300 μs difference). If Scheme 1 were an adequate description of the behavior of these channels, then the parameters of this model should fit the data over the full range of times and ATP concentrations. To compare the predictions to the actual traces over a wide range we averaged points on logarithmically spaced intervals to remove redundancy and noise and then overlaid the data with the predictions of the global fitting model (Fig. 10 B). There were three clear discrepancies. First, Scheme 1 predicts that the currents should rise more rapidly at high ATP concentration than the measured data. Second, the currents in response to low concentrations of ATP were substantially larger than predicted by the model. Third, the currents at times >100 ms, although small, were much larger than predicted by this model.

One trivial possible explanation for why the observed currents rose later than predicted was that we had overfiltered the data. However, exactly the same filter was applied to the response to the NMDG pulse and the ATP pulse, so any time shift should cancel out. A second possibility is that the appearance of ATP at the patch is delayed far longer than predicted by the diffusion convection model of the switching shown in Fig. 3, so that the time course of the response to NMDG is not an accurate indicator of when ATP is present. We tested this

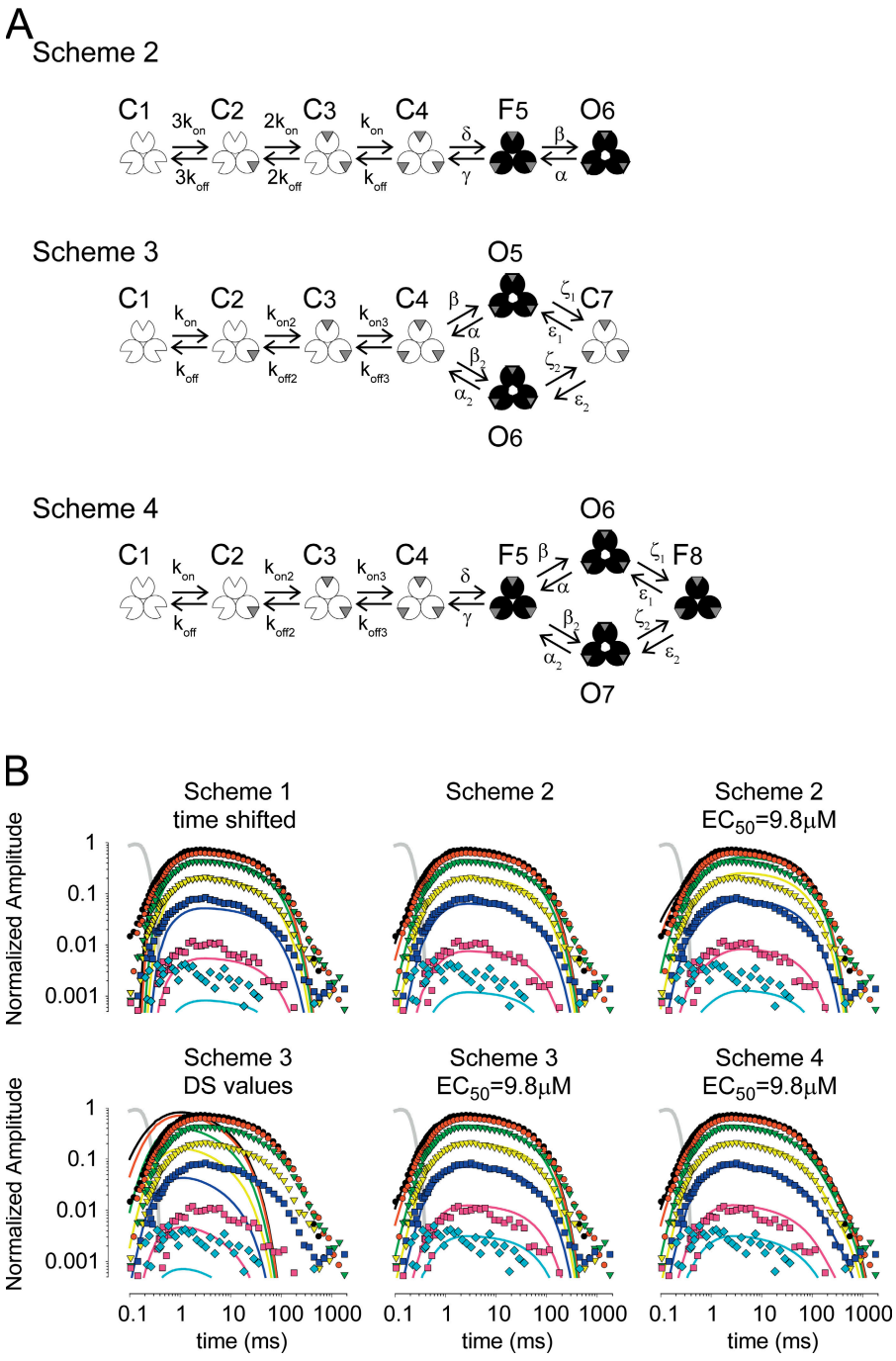

Figure 11. Further kinetic analysis. Comparison of experimental data with predictions of Schemes 2–4. (A) Schemes 2–4. Scheme 2 is a modification of Scheme 1 in which one additional closed state (the flip state) was added between the fully liganded channel and the open state. Scheme 3 is the preferred model of Ding and Sachs (1999). Scheme 4 inserts a flipped state into Scheme 3. (B) Global fit to the data generated by the different schemes. For time-shifted Scheme 1, a delay in the time of the drug application was included as an extra parameter in the global fit. The rationale was to mimic possible artifacts introduced by the drug application method. For the indicated schemes, the fit was forced to obey an EC_{50} of 9.8. For Scheme 3 we provide the prediction of the kinetic values obtained in the Ding and Sachs study. The solid lines are specific to each model, but the data points are identical in all panels.

possibility by modeling. We added an additional parameter to be optimized in the global fitting model, which represented a fixed delay until the ATP appeared. Not surprisingly, this succeeded in predicting the delay and rise time within the experimental error, something that Scheme 1 alone failed to do. However, this time-shifted version of Scheme 1 (Fig. 11 B) did a poorer job than the original Scheme 1 at predicting the responses at early times to high agonist concentration.

As technical artifacts could not account for the failure of Scheme 1, we expanded our modeling to include additional states. We used two alternative strategies: (1) to find a kinetic scheme that minimizes the number of states and connections between them, following a previous study by Ding and Sachs (1999) or (2) the strategy used by Horrigan and Aldrich (2002) "to define the simplest mechanism rather than the gating scheme with the fewest kinetic states that can account for the data."

The first strategy led to the analysis of Schemes 2, 3, and 4; the second to the allosteric Schemes 5–7, detailed in the next section. In Scheme 2, the channel does not begin to open immediately after the third subunit is filled

TABLE II

Results of the Least Squares Nonlinear Fitting of the Data under Schemes 2–7

Scheme	2 (EC_{50} free)	2	3	4	5	6	7
Df	6	6	13	15	7	15	15
SS (pA^2)	90, 512	960, 362	83,500	47,205	324,371	51,071	53,187
Macroscopic parameters							
EC_{50} (μM)	44.9			Constrained to 9.8 μM			
pO_{max}	0.0145	0.0032	0.109	0.158	0.985	0.54	0.92
pO_{min}	0	0	0	0	7×10^{-6}	0.004	0.0004
Kinetic rates							
k_{on} ($s^{-1}\mu M^{-1}$)	10.2 ± 11%	7.90 ± 12%	18.0 ± 81%	15.98 ± 120%	5.85 ± 11%	9.28 ± 17%	12.0 ± 24%
k_{on2} ($s^{-1}\mu M^{-1}$)			16.8 ± 64%	16.3 ± 85%			
k_{on3} ($s^{-1}\mu M^{-1}$)			8.42 ± 52%	11.6 ± 120%			
k_{off} (s^{-1})	1,869 ± 39%	121 ± 24%	0.017 ± 250%	0.019 ± 560%	190 ± 10%	1,871 ± 62%	6,731 ± 65%
k_{off2} (s^{-1})			175 ± 56%	380 ± 120%			
k_{off3} (s^{-1})			4,541 ± 30%	6,822 ± 61%			
γ (s^{-1})	27.9 ± 9%	42.1 ± 23%		43.54 ± 98%		1.07 ± 105%	242 ± 75%
δ (s^{-1})	3,491 ± 17%	632 ± 9%		3,718 ± 17%		3,875 ± 33%	9,035 ± 11%
α (s^{-1})	1,829 ± 9%	110,104 ± ∞%	29.0 ± 13%	1,088 ± 33%	10.2 ± 53%	776 ± 120%	110 ± 66%
α_2 (s^{-1})			1,189 ±410%	0.246 ±123%			
β (s^{-1})	27.3 ± 14%	382 ± ∞%	24.08 ± ∞%	540 ± 99%	769 ± 7%	914 ± 110%	1,380 ± 9%
β_2 (s^{-1})			3,198 ± 18%	0.033 ± 160%			
ε_1 (s^{-1})			1,936 ± 7%	79.0 ± 84%			
ε_2 (s^{-1})			8.48 ± 822%	3.20 ± 491%			
ζ_1 (s^{-1})			0.298 ± 680%	31.16 ± 123%			
ζ_2 (s^{-1})			$5.9*10^7$ ± 490%	4.53 ± 113%			
Allosteric factors							
A_{koff}					49.6 ± 17%	1.00 ± 34%	0.309 ± 316%
A_{kon}					4.51 ± 31%	1.77 ± 31%	1.00 ± 182%
A_{α}					48.9 ± 19%	2.30 ± 103%	1.00 ± 106%
A_{β}					4.58 ± 41%	0.77 ± 121%	0.309 ± 226%
B_{koff}						65.1 ± 72%	4,295 ± 270%
B_{kon}						1.15 ± 110%	1.00 ± 520%
B_{δ}						33.3 ± 115%	4,300 ± 260%
B_{γ}						2.25 ± 33%	1.00 ± 300%
C_{α}						0.19 ± 230%	10.1 ± 240%
C_{β}						635 ± ∞%	62.1 ± 380%
C_{δ}						1.00 ± ∞%	5.31 ± 440%
C_{γ}						123 ± 300%	118 ± 250%

The EC_{50} was forced to be 9.8 μM for all fits except for the version of Scheme 2 indicated as EC_{50} free. The data set is the same illustrated in Fig. 11. Df indicates the number of free parameters to be optimized by the nonlinear algorithm. SS indicates the sum of squared residuals. Except for Scheme 2 there was very little increase in the SS as a result of fixing the EC_{50}. The macroscopic parameters pOmax (maximum open probability for a saturating pulse of ATP) and pOmin (the open probability with no ATP present) were calculated based on the microscopic rates from each fit shown below. The EC_{50} was also calculated for Model 2. Standard errors of the estimated kinetic rates and allosteric constants were calculated on a logarithmic scale and presented as percentages. They were obtained using a bootstrap approach (Kraushaar and Jonas, 2000).

The kinetic rates of the fits are defined as follows. For Schemes 2, 5, 6, and 7 there was a single binding rate (k_{on}) and unbinding rate (k_{off}), while for Schemes 3 and 4 there were three independent rates designated as k_{on}, k_{on2}, and k_{on3} for binding and k_{off}, k_{off2}, and k_{off3} for unbinding. When flipping was present, the flipping rate was designated as δ and the unflipping rate as γ. β is the opening rate and α the closing rate from the fully liganded (and if relevant, fully flipped) state. For Schemes 3 and 4, additional values are provided for the opening to (β_2) and closing from (α_2) a second open state. For models 3 and 4 in which there are two open states, ζ is the rate of closing to, and ε the rate of opening from, a final closed state from which only opening is possible. The subscript 1 or 2 indicates the identity of the open state involved in the transition.

Allosteric factors of Schemes 5–7 are designated as follows. Binding–gating coupling factors start with an A. A_{kon} indicates the factor of increase in the binding rate produced by each ligand. A_{koff} indicates the factor of decrease in the unbinding rate per ligand. A_{α} indicates the factor of decrease in the closing rate per ligand and A_{β} the factor of increase in the opening rate per ligand. Binding–flipping coupling factors start with a B. B_{kon} is factor of increase in the binding rate to the binding domain produced by flipping of the whole channel (Scheme 6) or by the flipping of the same domain referred by the binding rate. B_{koff} is the factor of decrease in the unbinding rate produced by the flipping of the whole channel or of the relevant domain. B_{γ} and B_{δ} in Scheme 6 are the factor of increase and decrease of the flipping and unflipping rate produced by each ligand. In Scheme 7 they are the factor of increase and decrease of the flipping and unflipping rates produced at the ligand domain by the presence of a bound ligand. Flipping–gating coupling factors start with a C. C_{δ} and C_{γ} indicate the factor of increase in flipping rate and decrease in unflipping rate produced by the opening of the channels, whereas C_{β} and C_{α} indicate the factor of increase in opening and of decrease in closing produced by the flipping either of the whole channel (Scheme 6) or by each flipping domain (Scheme 7).

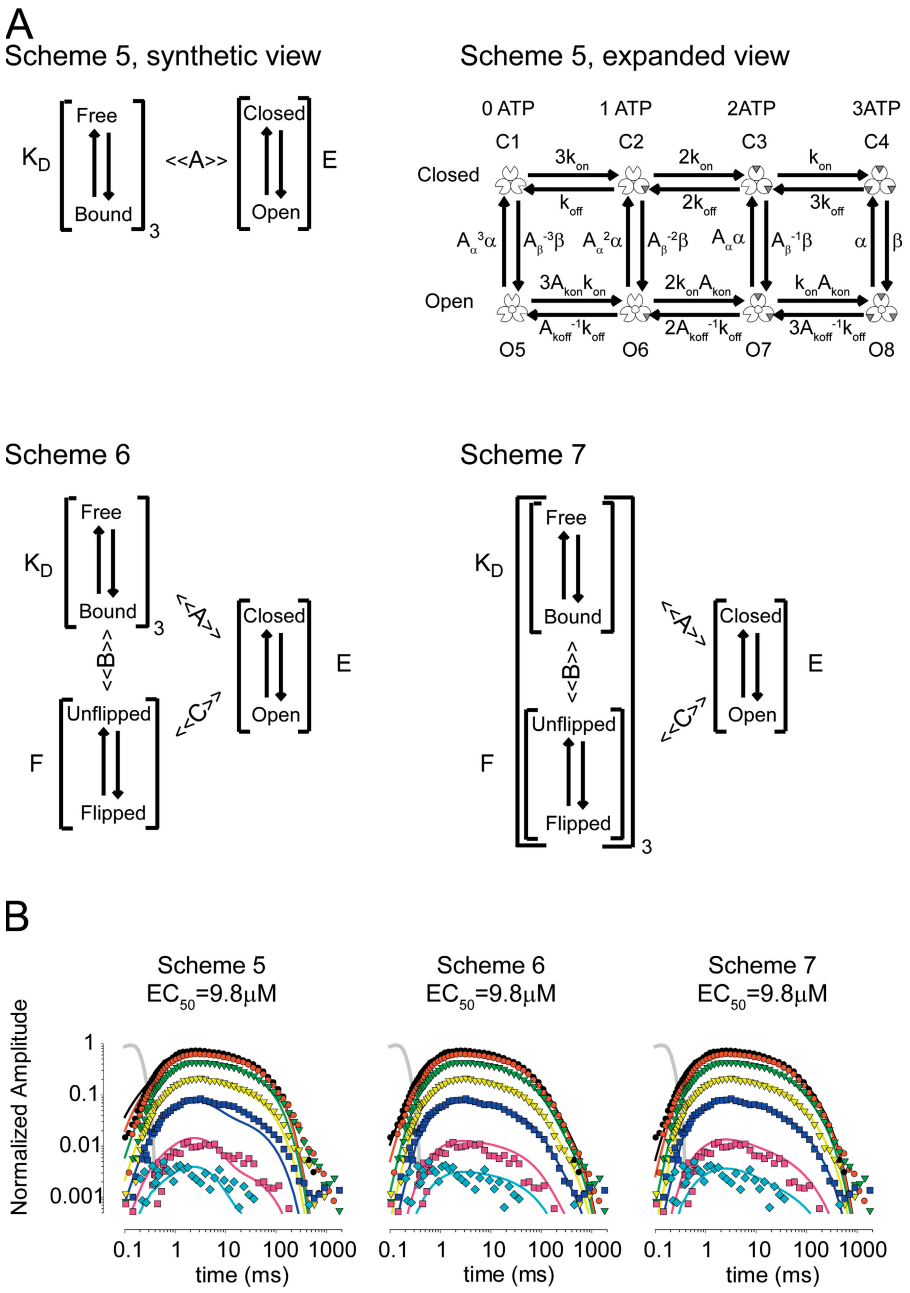

Figure 12. Allosteric analysis. (A) Schemes 5–7. Scheme 5 is the Monod-Wyman-Changeux model for a channel with three independent binding sites and, therefore, the allosteric extension of Scheme 1. Scheme 5 considers the allosteric interaction of two components: the binding sites and the gate. Each binding site can be either free or bound and the gate can be either closed or open. The expanded view shows the six states of the scheme and the formulas for the kinetic rates in terms of eight parameters: the same four kinetic rates of Scheme 1 (the binding and unbinding constants k_{on} and k_{off} and the opening and closing rates β and α) and the rate allosteric factors for each one of them (A_{kon}, A_{koff}, A_α, A_β). Scheme 6 is the allosteric expansion of Scheme 2; it includes flipping as a third component and it considers three allosteric couplings: binding–gating, binding–flipping, and flipping–gating. The expanded view is in Fig. S1. Scheme 7 is an alternative to Scheme 6 where flipping occurs independently at each binding site. The expanded view is presented in Figs. S2 and S3. (B) Global fits (solid lines) to the data (identical in all panels) using allosteric Schemes 5–7. Fits were forced to obey an EC_{50} of 9.8.

but rather has to pass through an intermediate closed state F5, which, following (Colquhoun and Sivilotti, 2004), we call a flipped state. Scheme 3 is the preferred scheme found by Ding and Sachs (1999); it branches into two open states that converged on a final closed state. Scheme 4 branches in the same way, but from the flipped state. Results for Schemes 2–4 are illustrated in Fig. 11 B and the optimized parameters are presented in Table II. For each scheme we also provide the predicted value of the macroscopic parameters EC_{50} and minimal and maximal open probability. A detailed discussion on the performance of Schemes 2 and 3 is available in the online supplemental material (available at http://www.jgp.org/cgi/content/full/jgp.200709779/DC1).

Scheme 4 fit the data well over the full range of concentrations and times. However, from a mechanistic point of view it is rather complex. First, Scheme 4 considers that the binding and unbinding rates are dependent on the number of molecules already bound. Since binding sites are likely to be far apart in the receptor, this suggests the presence of additional conformational changes associated with changes in the occupancy of the binding sites. The nature and kinetics of these conformational changes are not addressed by Scheme 4. Second, in Scheme 4 the channel can only open after the three binding sites are occupied and the channel has entered into the flipped state. In mechanistic terms, this is the same as saying that there is an "infinite" coupling

between binding and flipping and between flipping and gating. Third, Scheme 4 considers two open states and two flipped states; we need a mechanism for explaining the difference between them. We also need a mechanism to prevent the channel from going from F8 to C4. Taking into account these mechanistic complexities, we turned to allosteric models (Monod et al., 1965) of channel function as a potential alternative approach.

MWC Models of Channel Gating

The simplest allosteric model of channel function follows the model proposed by Monod, Wyman, and Changeux (1965) for the cooperative oxygen binding of hemoglobin. The MWC model can be applied to the behavior of the whole channel in terms of the simple interaction of two components: the binding sites and the gate. Each binding site can be either bound or free and the gate can be either open or closed. Each occupied binding site stabilizes the gate in the open position by the same amount. Conversely, the open channel stabilizes each binding site in the occupied state. When all bindings site are free, the gate is nearly always closed. After an agonist molecule is bound, the presence of the molecule at the binding site stabilizes the gate in the open conformation; with a sufficient number of agonist molecules bound, the gate is frequently open. The energy for stabilizing the open conformation comes from an increased affinity for each molecule of bound agonist. Therefore, the opening of the channel involves a concerted movement of the whole protein, trapping the agonist at a higher affinity at the same time as allowing the passage of ions through the pore.

At equilibrium, the distribution of the channel among the states of this simple allosteric model can be predicted by three constants. K_D is the dissociation constant of ATP from the closed state (K_{off}/K_{on}), E is the efficacy of channel opening when ATP is bound to all sites (β/α), and A is the allosteric constant. The allosteric constant *A* indicates the factor that the affinity for the agonist induced by the opening of the channel increases as well as the factor that the efficacy of the channel increases by the binding of a single molecule of agonist.

For a homomeric, multisubunit protein like $P2X_2$ receptors, the individual kinetic rates are functions of *s*, the state of the gate ($s = 0$ for closed and $s = 1$ for open), and *n*, the number of bound domains of the starting state of the rate constant (0–2 for binding, 1–3 for unbinding). As shown in the expansion of Scheme 5 represented in Fig. 12 A, to convert this allosteric model to a kinetic model it is necessary to define 20 rates. However, only seven parameters are required. Four of them are the same parameters of Scheme 1, k_{on}, k_{off}, β, and α; the other three parameters are allosteric rate factors. The allosteric constant A can be expressed as the product of individual allosteric rate factors, where A_{kon} indicates the factor of increase in the binding rate produced by each ligand, A_{koff} indicates the factor of decrease in the unbinding rate per ligand, A_α indicates the factor of decrease in the closing rate per ligand, and A_β the factor of increase in the opening rate per ligand. With these definitions, microscopic reversibility requires that $A = A_{kon} \cdot A_{koff} = A_\beta \cdot A_\alpha$ so only three of these four factors are free parameters.

Binding or unbinding rates are thus:

$$k_{on}(s,n) = (3-n) \cdot A_{kon}{}^{s} \cdot k_{on} \tag{6}$$

$$k_{off}(s,n) = n \cdot \frac{k_{off}}{A_{koff}{}^{s}}, \tag{7}$$

where k_{off} and k_{on} represent the microscopic rate constant for the closed channel. If we assume that each binding domain acts independently of the others, the opening and closing rates are

$$\beta(n) = \beta \cdot A_\beta{}^{n-3} \tag{8}$$

$$\alpha(n) = \frac{\alpha}{A_\alpha{}^{n-3}}, \tag{9}$$

where $\beta(n)$ is the opening rate of the *n*-bound channel and $\alpha(n)$ the closing rate of the *n*-bound channel (we define $\alpha = \alpha(3)$ and $\beta = \beta(3)$, in order to allow an easy comparison with Schemes 1–4).

We used the nonlinear algorithm described in detail in the online supplemental material to optimize the value of the kinetic rates (Table II, Scheme 5). However, this scheme clearly failed to predict the early rise of the current as well as the late decay (Figure. 12 B, Scheme 5). This did not come as a surprise, since the scheme lacks an extra state between fully bound and the open state. It also fails to predict the late decay of the current. If we let all 20 rates be free (but required them to obey microscopic reversibility), we found a better description of the late decay but not of the early rise of the current (unpublished data).

Flipping Allosteric Models of Channel Gating

As the two-component MWC allosteric model for these channels failed, we switched to allosteric models incorporating an additional conformational change: flipping. As far as we know, P2X receptors have only one gate and three binding sites. How many flipping units do they have? They might have only one flipping unit, if the protein flips as a whole, or they can have three flipping units, if each binding domain flips in its own. These two possibilities are described by Schemes 6 and 7 (Fig. 12 A).

The global flipping scheme (Fig. 12 A, Scheme 6) can be thought of as if all the flipping domains were subject to tight interactions, so they only move in a concerted fashion. In Fig. S2 we show this scheme fully expanded to its standard representation: it comprises four closed

unflipped states (C_1–C_4), four closed flipped states (F_5–F_8), and the eight open versions of them all (O_9–O_{16}). In this scheme, the flipping ratio increases exponentially with the number of occupied binding sites and the opening ratio increases in the flipped state. This scheme is analogous to the mechanism postulated by the Colquhoun group recently for heteromeric glycine receptors (Burzomato et al., 2004), although the scheme presented here considers more states and connections.

In the localized flipping scheme (Fig. 12 A, Scheme 7), each binding domain flips independently and it is coupled allosterically to its occupancy state. It comprises 40 states (Figs. S3 and S4): four closed unflipped states (C1–C4 with 0–3 bound agonist), six single-flipped states (F5–F10), six double-flipped states (F11–F16), and four triple-flipped states (F17–F20) and the 20 open versions of them (O21–O40). The gate is allosterically coupled to the flipped domains. The opening rate increases exponentially with the number of flipped domains (Fig. S2). This scheme is analogous to the postulated mechanisms of coupling of voltage sensor activation and Ca^{2+} binding in the BK channel in which the interaction occurs only in the same subunit (Horrigan and Aldrich, 2002). In this scheme, there is no coupled movement of the channel; the opening of the gate results from the independent contribution of each flipping unit.

Global analyses were performed and the least square algorithm converged for both Schemes 6 and 7. Both schemes did an excellent job of reproducing the data obtained for responses to ultrabrief pulses at durations up to 800 ms, but poorly predicted the residual current at longer times (Fig. 12 B, Schemes 6 and 7). None of the explored schemes predicted the desensitization found after hundreds of milliseconds.

DISCUSSION

At many chemical synapses the vesicular release mechanism produces a very brief pulse of neurotransmitter that transiently achieves a high local concentration at the postsynaptic receptors. To explore the consequences of a brief appearance of ATP at purinergic synapses, we developed methods that allowed us to apply and remove ATP from patches expressing $P2X_2$ receptors within 200 μs. In previous studies of this type on glutamate, GABA, and ACh receptors (Colquhoun et al., 1992; Franke et al., 1992; Dzubay and Jahr, 1996), the speed of solution exchange was assessed by measuring the junction potential produced by solutions of different composition when the patch was ruptured at the end of the experiment. We found that this was not an adequate test of the speed of exchange, as it was common to find patches that gave quite slow responses to ATP concentration jumps even though the speed of the subsequent junction potentials indicated that the recording and drug application pipettes were optimally positioned for fast exchange. It seems likely that the slow patches had folded back onto themselves and produced an extra barrier to diffusion. To deal with this problem, we developed a calibration method that can be applied to intact patches. This general approach to measuring solution exchange time (changing the permeant ions without changing channel gating) should probably be applied in all future experiments of this type, regardless of the specific ligand and receptor under study.

Physiological Implications

Our rationale for carrying out these experiments was that rapidly applying ATP to outside-out patches expressing $P2X_2$ receptors would allow us to gain insight into the way that $P2X_2$ receptors localized at synapses might function. Are there in fact synapses that use $P2X_2$ receptors? Light level immunohistochemistry has demonstrated that the $P2X_2$ protein is widely expressed in the mammalian central nervous system (Kanjhan et al., 1999), and immunoelectron microscopy has demonstrated the presence of $P2X_2$ subunits at synapses in the cerebellum and hippocampus (Rubio and Soto, 2001) and in the retina (Puthussery and Fletcher, 2006). There is physiological evidence for purinergic synaptic signaling in all three of these regions of the CNS (Burnstock, 2007) but because of the absence of subunit-specific antagonists and because $P2X_2$ subunits readily form heteromeric complexes with other P2X subunits, this is insufficient evidence to conclude that homomeric $P2X_2$ receptors are present at these synapses. Indeed, in systems involved in pain sensation (Cockayne et al., 2005) and taste sensation (Finger et al., 2005) both the $P2X_2$ and $P2X_3$ genes need to be knocked out in order to produce a large diminution in the sensory response, suggesting that homomeric $P2X_2$ and $P2X_3$ receptors may be rare in these sensory cells. In contrast, most sympathetic neurons from $P2X_2$ knockout mice have virtually no response to exogenous ATP, suggesting that their normal responses are dominated by homomeric $P2X_2$ receptors (Cockayne et al., 2005). Most relevant of all, S type myenteric neurons, which normally receive fast excitatory postsynaptic potentials (EPSPs) that have a cholinergic and a purinergic component, have no detectable purinergic component to the fast EPSP in $P2X_2$ knockout mice (Ren et al., 2003). As all P2X receptor subunits (with the possible exception of $P2X_6$) can form functional homomeric receptors, the implication of this work is that the purinergic component at these synapses is due exclusively to homomeric $P2X_2$ receptors. Given that $P2X_2$ receptors are present at synapses, is the ATP transient fast? Recent work suggests that ATP release from glial cells (Cotrina et al., 2000; Stout et al., 2002) and from rodent taste receptor cells (Huang et al., 2007; Romanov et al., 2007) may be through connexin or pannexin hemichannels; the kinetics of this type of release

mechanism is unknown. However, the release of ATP from neurons in the mouse cortex appears to be by conventional fast calcium-dependent exocytosis (Pankratov et al., 2007) as does ATP release onto the S type myenteric neurons.

Another important question is how similar the kinetics of the ATP responses we measured in patches are to responses of $P2X_2$ receptors present at synapses. This is of concern because a number of factors, including channel density, patch excision, and the level of extracellular calcium, are known to dramatically alter the properties of these receptors.

The density of channels in patches and whole cells can be estimated by dividing the peak current by the estimated surface area, and then scaling the result by the single channel current and the maximum open probability. This yields an estimate of ~100 channels per μm^2 in our patches, but an average density of only 0.5–5 channels per μm^2 in dissociated neurons from superior cervical ganglia, dorsal root ganglia, and nodose ganglia (Cockayne et al., 2005). At low expression levels, $P2X_2$ receptors expressed in oocytes have a high EC_{50} (Clyne et al., 2003), and ATP is less likely to trigger the megapore state that allows large cations like NMDG to permeate the membrane (Fujiwara and Kubo, 2004). The likely single channel manifestation of these density-dependent effects is that when a patch contains more than one functional channel, it is common to see non-independent gating and the kinetic properties of the channels in these patches are quite different from patches with only one channel (Ding and Sachs, 2002). The observation that nonindependent gating appears when as few as two channels are in a patch (Ding and Sachs, 2002) suggests that channels have a high prosperity to interact with each other whenever possible. Theobservation that once the peak current per oocyte exceeds 10 μA (which corresponds to less than six channels per μm^2) the effect of channel density on the EC_{50} has saturated (Clyne et al., 2003) supports the same interpretation. Furthermore, $P2X_2$ receptors are known to be clustered on the cell surface (Khakh et al., 2001; Ren et al., 2003), especially at synapses. Therefore $P2X_2$ receptors at synapses are likely to be in the high density state, as are the receptors in our patches.

A second issue of relevance to the properties of the channels we studied is that we performed our experiments in the presence of 1 mM magnesium, but with no external calcium, while both calcium and magnesium would be present at millimolar levels at synapses in vivo. The rationale for this choice was that $P2X_2$ currents in outside-out patches desensitize much more rapidly than $P2X_2$ currents from intact cells (Zhou and Hume, 1998). Recent work suggests that the loss of membrane-bound phosphoinositides may be responsible for the change in channel properties following patch excision (Fujiwara and Kubo, 2006). This accelerated desensitization was also demonstrated to depend on extracellular calcium (Ding and Sachs, 2000). Furthermore, the steady-state desensitization of outside-out patches exposed to millimolar calcium is much more extensive (reaching nearly 100%) than for intact cells, and the recovery from desensitization has a half time of nearly 10 min, meaning that these patches are unable to respond at all to a second application of ATP for several minutes. In contrast, purinergic synapses on myenteric neurons show no such rundown. By eliminating extracellular calcium from the recording solution, we were able to produce steady-state responses in outside-out patches that more closely matched the responses of intact cells, and to observe many ATP responses from a single patch. Thus $P2X_2$ receptors in outside-out patches have properties most similar to the endogenous receptors when they are studied in the absence of calcium. However, it must be recognized that the receptors in these patches are unlikely to behave identically to channels present at synapses, so the detailed kinetic modeling we have performed should be regarded as providing only the best available information as to how synaptic receptors would behave.

A striking observation of the current study was the relatively slow activation and very slow deactivation of $P2X_2$ receptors in outside-out patches. For ATP pulses of 0.2 ms, most channel openings occurred after the free ATP concentration had fallen back to 0, with the peak response occurring at ~4 ms and the full response lasting for >500 ms. These properties stand in great contrast to AMPA type glutamate receptors, which are also nonselective cation channels, but respond very rapidly to the appearance and disappearance of glutamate (Colquhoun et al., 1992). The kinetic properties of $P2X_2$ receptors much more closely resemble the properties of the NMDA receptors found at glutamatergic synapses (Dzubay and Jahr, 1996). Interestingly, NMDA receptors and $P2X_2$ receptors are both calcium permeable (MacDermott et al., 1986; Mayer and Westbrook, 1987; Evans et al., 1996) and modulated by extracellular pH and extracellular zinc. However, the modulation is oppositely directed, with elevated zinc or protons inhibiting NMDA receptors (Westbrook and Mayer, 1987; Tang et al., 1990; Traynelis and Cull-Candy, 1990), but potentiating $P2X_2$ receptors (Wildman et al., 1998; Clyne et al., 2002). Similarly, membrane potential also has opposite effects, with depolarization inhibiting $P2X_2$ receptors due to voltage-dependent gating (Zhou and Hume, 1998) while depolarization increases current through NMDA receptors due to a decrease in magnesium binding in the pore (Mayer et al., 1984). Thus, $P2X_2$ receptors have properties capable of producing a substantial synaptically gated calcium influx under conditions under which NMDA receptors are nonfunctional. The voltage-dependent gating of NMDA receptors is essential for the computations performed by circuits involved in learning and forgetting (Xia et al., 1996).

$P2X_2$ receptors are very widely expressed in the mammalian central nervous system (North, 2002), and it will be of great interest to determine whether the modulations by membrane potential and by binding ions also play a special role in the computations of the neurons that express them.

Kinetic Modeling of $P2X_2$ Receptor Currents

Our modeling approach was guided by two highly relevant sets of previous results. Ding and Sachs (1999) performed a single channel analysis of $P2X_2$ receptor currents in single channel patches. We therefore attempted to fit our data with their preferred kinetic scheme that requires all three agonist binding sites to be occupied in order for channels to open (Scheme 3). Our experimental approach differs from theirs because we knew the time of appearance of ATP at the channels, while their approach was based on studying channels opening and closing with a steady concentration of ATP present. We therefore had the potential to discover kinetic information that was not available in the previous study.

The second modeling approach was motivated by recent studies suggesting that although glycine α subunits can form homopentameric receptors, not all agonist sites need to be occupied to get a maximal effect (Gentet and Clements, 2002; Beato et al., 2004). Colquhoun and Silvilotti (2004) speculated that "after three of the M2 domains of the α subunits have rotated, and broken out of the side-to-side bonds in the hydrophobic gate, this ring is destabilized as much as possible." We thought it possible that the trimeric $P2X_2$ receptors might open with fewer than three bound ATP, because heteromeric $P2X_2/P2X_3$ receptors can open in response to α,β methylene ATP, an agonist that produces little or no response in $P2X_2$ receptors. Opening from the less then fully liganded state is a natural property of MWC type models of channel gating.

For two reasons it was not expected that the parameters reported by Ding and Sachs (1999) from patches with very few channels would describe our data. First, $P2X_2$ receptors are voltage dependent (Zhou and Hume, 1998) and we used a different holding potential than in the Ding and Sachs study. Second, we studied receptors at high density, and several studies have indicated that the properties of $P2X_2$ receptors change as density increases (Ding and Sachs, 2002; Clyne et al., 2003; Fujiwara and Kubo, 2004). We therefore allowed our fitting algorithm to select the optimal parameters. Scheme 3 predicts that at sufficiently high ATP concentration, channel opening should be virtually instantaneous, but we found that there was a measurable delay between when ATP arrives and when currents can be detected. One simple way to account for this delay is to postulate an additional closed state interposed between the triply liganded state and the open state (Scheme 4). By analogy to recent work on glycine receptors, we refer to this hypothesized state as a flipped state. Introducing a flipped state into a model without allosteric interactions (Scheme 2) was not able to reproduce our data, but two very different types of allosteric models with a flipped state fit the data well. In Scheme 4, there is highly significant cooperativity between each binding step, while in Schemes 6 and 7, there is negligible cooperativity of binding. Rather, the major allosteric coupling is between binding and flipping or flipping and opening. A specific prediction of the MWC models is that the rate of opening of partially liganded receptors is not zero. By analogy to studies of nicotinic acetylcholine receptors, it might be easiest to further explore this issue in mutant receptors that have increased efficacy.

We thank members of the Hume laboratory for critical reading of the manuscript. Computational resources were provided by the Center for the Study of Complex Systems, University of Michigan.

This work was supported by National Institutes of Health grant NS039196 (R.I. Hume) and by Agencia Nacional de Promoción Científica y Técnológica PICT 06-12345 (L. Moffatt).

Olaf S. Andersen served as editor.

Submitted: 8 March 2007
Accepted: 13 July 2007

REFERENCES

Banke, T.G., and S.F. Traynelis. 2003. Activation of NR1/NR2B NMDA receptors. *Nat. Neurosci.* 6:144–152.

Barry, P.H., and J.W. Lynch. 1991. Liquid junction potentials and small cell effects in patch-clamp analysis. *J. Membr. Biol.* 121:101–117.

Bartoletti, S., B.D. Flury, and D.G. Nel. 1999. Allometric extension. *Biometrics.* 55:1210–1214.

Beato, M., P.J. Groot-Kormelink, D. Colquhoun, and L.G. Sivilotti. 2004. The activation mechanism of α1 homomeric glycine receptors. *J. Neurosci.* 24:895–906.

Brooks, S.P., and K.B. Storey. 1992. Bound and determined: a computer program for making buffers of defined ion concentrations. *Anal. Biochem.* 201:119–126.

Burnstock, G. 2007. Physiology and pathophysiology of purinergic neurotransmission. *Physiol. Rev.* 87:659–797.

Burzomato, V., M. Beato, P.J. Groot-Kormelink, D. Colquhoun, and L.G. Sivilotti. 2004. Single-channel behavior of heteromeric α1β glycine receptors: an attempt to detect a conformational change before the channel opens. *J. Neurosci.* 24:10924–10940.

Clyne, J.D., L.D. LaPointe, and R.I. Hume. 2002. The role of histidine residues in modulation of the rat P2X2 purinoceptor by zinc and pH. *J. Physiol.* 539:347–359.

Clyne, J.D., T.C. Brown, and R.I. Hume. 2003. Expression level dependent changes in the properties of P2X2 receptors. *Neuropharmacology.* 44:403–412.

Cockayne, D.A., P.M. Dunn, Y. Zhong, W.F. Rong, S.G. Hamilton, G.E. Knight, H.Z. Ruan, B. Ma, P. Yip, P. Nunn, et al. 2005. P2X(2) knockout mice and P2X(2)/P2X(3) double knockout mice reveal a role for the P2X(2) receptor subunit in mediating multiple sensory effects of ATP. *J. Physiol.* 567:621–639.

Colquhoun, D., and L.G. Sivilotti. 2004. Function and structure in glycine receptors and some of their relatives. *Trends Neurosci.* 27:337–344.

Colquhoun, D., P. Jonas, and B. Sakmann. 1992. Action of brief pulses of glutamate on AMPA/kainate receptors in patches from different neurones of rat hippocampal slices. *J. Physiol.* 458:261–287.

Cotrina, M.L., J.H. Lin, J.C. Lopez-Garcia, C.C. Naus, and M. Nedergaard. 2000. ATP-mediated glia signaling. *J. Neurosci.* 20:2835–2844.

Diamond, J.S. 2001. Neuronal glutamate transporters limit activation of NMDA receptors by neurotransmitter spillover on CA1 pyramidal cells. *J. Neurosci.* 21:8328–8338.

Ding, S., and F. Sachs. 1999. Single channel properties of P2X2 purinoceptors. *J. Gen. Physiol.* 113:695–719.

Ding, S., and F. Sachs. 2000. Inactivation of P2X(2) purinoceptors by divalent cations. *J. Physiol.* 522:199–214.

Ding, S., and F. Sachs. 2002. Evidence for non-independent gating of P2X2 receptors expressed in *Xenopus* oocytes. *BMC Neurosci.* 3:17.

Dzubay, J.A., and C.E. Jahr. 1996. Kinetics of NMDA channel opening. *J. Neurosci.* 16:4129–4134.

Evans, R.J., C. Lewis, C. Virginio, K. Lundstrom, G. Buell, A. Surprenant, and R.A. North. 1996. Ionic permeability of, and divalent cation effects on, two ATP-gated cation channels (P2X receptors) expressed in mammalian cells. *J. Physiol.* 497:413–422.

Finger, T.E., V. Danilova, J. Barrows, D.L. Bartel, A.J. Vigers, L. Stone, G. Hellekant, and S.C. Kinnamon. 2005. ATP signaling is crucial for communication from taste buds to gustatory nerves. *Science.* 310:1495–1499.

Franke, C., D. Koltgen, H. Hatt, and J. Dudel. 1992. Activation and desensitization of embryonic-like receptor channels in mouse muscle by acetylcholine concentration steps. *J. Physiol.* 451:145–158.

Fujiwara, Y., and Y. Kubo. 2004. Density-dependent changes of the pore properties of the P2X2 receptor channel. *J. Physiol.* 558:31–43.

Fujiwara, Y., and Y. Kubo. 2006. Regulation of the desensitization and ion selectivity of ATP-gated P2X2 channels by phosphoinositides. *J. Physiol.* 576:135–149.

Gentet, L.J., and J.D. Clements. 2002. Binding site stoichiometry and the effects of phosphorylation on human α1 homomeric glycine receptors. *J. Physiol.* 544:97–106.

Grewer, C. 1999. Investigation of the α1-glycine receptor channel-opening kinetics in the submillisecond time domain. *Biophys. J.* 77:727–738.

Hell, J.W., L. Edelmann, J. Hartinger, and R. Jahn. 1991. Functional reconstitution of the γ-aminobutyric acid transporter from synaptic vesicles using artificial ion gradients. *Biochemistry.* 30:11795–11800.

Horrigan, F.T., and R.W. Aldrich. 2002. Coupling between voltage sensor activation, Ca^{2+} binding and channel opening in large conductance (BK) potassium channels. *J. Gen. Physiol.* 120:267–305.

Huang, Y.J., Y. Maruyama, G. Dvoryanchikov, E. Pereira, N. Chaudhari, and S.D. Roper. 2007. The role of pannexin 1 hemichannels in ATP release and cell-cell communication in mouse taste buds. *Proc. Natl. Acad. Sci. USA.* 104:6436–6441.

Jayaraman, V., S. Thiran, and G.P. Hess. 1999. How fast does the γ-aminobutyric acid receptor channel open? Kinetic investigations in the microsecond time region using a laser-pulse photolysis technique. *Biochemistry.* 38:11372–11378.

Kanjhan, R., G.D. Housley, L.D. Burton, D.L. Christie, A. Kippenberger, P.R. Thorne, L. Luo, and A.F. Ryan. 1999. Distribution of the P2X(2) receptor subunit of the ATP-gated ion channels in the rat central nervous system. *J. Comp. Neurol.* 407:11–32.

Khakh, B.S., X.R. Bao, C. Labarca, and H.A. Lester. 1999. Neuronal P2X transmitter-gated cation channels change their ion selectivity in seconds. *Nat. Neurosci.* 2:322–330.

Khakh, B.S., W.B. Smith, C.S. Chiu, D.H. Ju, N. Davidson, and H.A. Lester. 2001. Activation-dependent changes in receptor distribution and dendritic morphology in hippocampal neurons expressing P2X(2)-green fluorescent protein receptors. *Proc. Natl. Acad. Sci. USA.* 98:5288–5293. (published erratum appears in *Proc. Natl. Acad. Sci. USA.* 2001. 98:7647)

Khakh, B.S., D. Gittermann, D.A. Cockayne, and A. Jones. 2003. ATP modulation of excitatory synapses onto interneurons. *J. Neurosci.* 23:7426–7437.

Kraushaar, U., and P. Jonas. 2000. Efficacy and stability of quantal GABA release at a hippocampal interneuron-principal neuron synapse. *J. Neurosci.* 20:5594–5607.

Land, B.R., W.V. Harris, E.E. Salpeter, and M.M. Salpeter. 1984. Diffusion and binding constants for acetylcholine derived from the falling phase of miniature endplate currents. *Proc. Natl. Acad. Sci. USA.* 81:1594–1598.

Li, G., W. Pei, and L. Niu. 2003. Channel-opening kinetics of GluR2Q(flip) AMPA receptor: a laser-pulse photolysis study. *Biochemistry.* 42:12358–12366.

Li, H., L.M. Nowak, K.R. Gee, and G.P. Hess. 2002. Mechanism of glutamate receptor-channel function in rat hippocampal neurons investigated using the laser-pulse photolysis (LaPP) technique. *Biochemistry.* 41:4753–4759.

MacDermott, A.B., M.L. Mayer, and G.L. Westbrook. 1986. NMDA-receptor activation increases cytoplasmic calcium concentration in cultured spinal cord neurones. *Nature.* 321:519–522.

Matsubara, N., A.P. Billington, and G.P. Hess. 1992. How fast does an acetylcholine receptor channel open? Laser-pulse photolysis of an inactive precursor of carbamoylcholine in the microsecond time region with BC3H1 cells. *Biochemistry.* 31:5507–5514.

Mayer, M.L., G.L. Westbrook, and P.B. Buthrie. 1984. Voltage-dependent block by Mg^{2+} of NMDA responses in spinal cord neurones. *Nature.* 309:261–263.

Mayer, M.L., and G.L. Westbrook. 1987. Permeation and block of *N*-methyl-D-aspartic acid receptor channels by divalent cations in mouse cultured central neurones. *J. Physiol.* 394:501–527.

Monod, J., J. Wyman, and J.P. Changeux. 1965. On nature of allosteric transitions—a plausible model. *J. Mol. Biol.* 12:88–118.

North, R.A. 2002. Molecular physiology of P2X receptors. *Physiol. Rev.* 82:1013–1067.

Pankratov, Y., U. Lalo, A. Verkhratsky, and R.A. North. 2007. Quantal release of ATP in mouse cortex. *J. Gen. Physiol.* 129:257–265.

Pankratov, Y.V., U.V. Lalo, and O.A. Krishtal. 2002. Role for P2X receptors in long-term potentiation. *J. Neurosci.* 22:8363–8369.

Popescu, G., and A. Auerbach. 2003. Model gating of NMDA receptors and the shape of their synaptic response. *Nat. Neurosci.* 6:476–483.

Puthussery, T., and E.L. Fletcher. 2006. P2X2 receptors on ganglion and amacrine cells in cone pathways of the rat retina. *J. Comp. Neurol.* 496:595–609.

Reid, C.A., J.M. Bekkers, and J.D. Clements. 1998. N- and P/Q-type Ca^{2+} channels mediate transmitter release with a similar cooperativity at rat hippocampal autapses. *J. Neurosci.* 18:2849–2855.

Ren, J., X.C. Bian, M. DeVries, B. Schnegelsberg, D.A. Cockayne, A. Ford, and J.J. Galligan. 2003. P2X(2) subunits contribute to fast synaptic excitation in myenteric neurons of the mouse small intestine. *J. Physiol.* 552:809–821.

Rogers, A.W., Z. Darzynkiewicz, E.A. Barnard, and M.M. Salpeter. 1966. Number and location of acetylcholinesterase molecules at motor endplates of the mouse. *Nature.* 210:1003–1006.

Romanov, R.A., O.A. Rogachevskaja, M.F. Bystrova, P. Jiang, R.F. Margolskee, and S.S. Kolesnikov. 2007. Afferent neurotransmission mediated by hemichannels in mammalian taste cells. *EMBO J.* 26:657–667.

Rubio, M.E., and F. Soto. 2001. Distinct localization of P2X receptors at excitatory postsynaptic specializations. *J. Neurosci.* 21:641–653.

Sachs, F. 1999. Practical limits on the maximal speed of solution exchange for patch clamp experiments. *Biophys. J.* 77:682–690.

Stiles, J.R., I.V. Kovyazina, E.E. Salpeter, and M.M. Salpeter. 1999. The temperature sensitivity of miniature endplate currents

is mostly governed by channel gating: evidence from optimized recordings and Monte Carlo simulations. *Biophys. J.* 77:1177–1187.

Stilson, S., A. McClellan, and S. Devasia. 2001. High-speed solution switching using piezo-based micropositioning stages. *IEEE Trans. Biomed. Eng.* 48:806–814.

Stout, C.E., J.L. Costantin, C.C. Naus, and A.C. Charles. 2002. Intercellular calcium signaling in astrocytes via ATP release through connexin hemichannels. *J. Biol. Chem.* 277:10482–10488.

Tang, C.M., M. Dichter, and M. Morad. 1990. Modulation of the *N*-methyl-D-aspartate channel by extracellular H^+. *Proc. Natl. Acad. Sci. USA.* 87:6445–6449.

Tong, G., and C.E. Jahr. 1994. Block of glutamate transporters potentiates postsynaptic excitation. *Neuron.* 13:1195–1203.

Traynelis, S.F., and S.G. Cull-Candy. 1990. Proton inhibition of *N*-methyl-D-aspartate receptors in cerebellar neurons. *Nature.* 345:347–350.

Virginio, C., A. MacKenzie, F.A. Rassendren, R.A. North, and A. Surprenant. 1999. Pore dilation of neuronal P2X receptor channels. *Nat. Neurosci.* 2:315–321.

Westbrook, G.L., and M.L. Mayer. 1987. Micromolar concentrations of Zn^{2+} antagonize NMDA and GABA responses of hippocampal neurons. *Nature.* 328:640–643.

Westfall, T.D., C. Kennedy, and P. Sneddon. 1996. Enhancement of sympathetic purinergic neurotransmission in the guinea-pig isolated vas deferens by the novel ecto-ATPase inhibitor ARL 67156. *Br. J. Pharmacol.* 117:867–872.

Wildman, S.S., B.F. King, and G. Burnstock. 1998. Zn^{2+} modulation of ATP-responses at recombinant P2X2 receptors and its dependence on extracellular pH. *Br. J. Pharmacol.* 123:1214–1220.

Xia, Z., H. Dudek, C.K. Miranti, and M.E. Greenberg. 1996. Calcium influx via the NMDA receptor induces immediate early gene transcription by a MAP kinase/ERK-dependent mechanism. *J. Neurosci.* 16:5425–5436.

Zafra, F., C. Aragon, L. Olivares, N. Danbolt, C. Gimenez, and J. Storm-Mathisen. 1995. Glycine transporters are differentially expressed among CNS cells. *J. Neurosci.* 15:3952–3969.

Zhou, Z., and R.I. Hume. 1998. Two mechanisms for inward rectification of current flow through the purinoceptor P2X(2) class of ATP-gated channels. *J. Physiol.* 507:353–364.